RC1

We thank the reviewer for his careful reading of the manuscript and attention to detail. These comments, and our responses as described below, improved the focus, clarity, and main points of the manuscript.

General Comments

Improved and more precise evaluation of turbulent exchange of momentum, energy, and passive and active chemical compounds between the land and the atmosphere in presence of vegetation canopy is beneficial for both modeling and measurement communities. This model development report quantifies the canopy and the roughness-sublayer (RSL) induced turbulent effects on surface-atmosphere exchange properties as evaluated by comparing large observational data, Community Land Model version 4.5(CLM4.5) and multi-layer canopy model. The authors concluded that 'the implementation of the RSL improves model performances in terms of sensible heat flux, friction velocity, and radiative temperature, and additional improvement comes from modeling stomatal conductance and canopy physiology beyond what is in the CLM4.5 .', which is important and relevant conclusion. The paper is well written and provides the all necessary information of the modeling system.

The main drawback of the paper however, is often not clear separation of the added value of the included RSL parameterization, and the 'Leaf biophysics' incorporation in the model, when presenting and discussing the results (although figures/tables show this clearly). For example, the conclusion sentence, cited above, states that the RSL improves the sensible heat flux, friction velocity and the radiative temperature. This is only true when taken the RSL together with the leaf biophysics improvement in the multi-layer approach, but not entirely true for the sensible and the latent fluxes as seen separately only for the RSL effects (we cannot know this since the RSL here is always linked to the leaf physics of the multi-layer model, and the latter is absent/different in the CLM).

Response: We revised this sentence to distinguish the effects of leaf biophysics from the RSL and further elaborated on this point: "*The multi-layer canopy improves model performance compared to the CLM4.5 in terms of latent and sensible heat fluxes, friction velocity, and radiative temperature. Improvement in latent and sensible heat fluxes comes primarily from advances in modeling stomatal conductance and canopy physiology beyond what is in the CLM4.5. These advances also improve friction velocity and radiative temperature, with additional improvement from the RSL parameterization. The multi-layer canopy combines improvements in both leaf biophysics and canopy-induced turbulence and both contribute to the overall model improvement.*"

page 2, line 29-30 in the abstract: please see the same comment in the general note. The effective influence of the RSL on presented quantities would be by comparing the ML-RSL and ML+RSL.

Response: We wrote this sentence to distinguish the effects of leaf biophysics from the RSL: "*Advances in modeling stomatal conductance and canopy physiology beyond what is in the CLM4.5 substantially improve model performance. The signature of the roughness sublayer is most evident in nighttime friction velocity and the diurnal cycle of radiative temperature, but is also seen in sensible heat flux.*"

page 8, Eq. 1, 2, 3, 4: The fluxes, as stated in the equations, show that they are height dependent (e.g. $dH/dz=f(z)$); but later (page 15, Eq. 18-20 are derived from $dc/dz = c_*/(kz)\Phi_c$ (e.g. Harman and Finnigan 2008, Eq. 12) on the assumption that the fuxes above the canopy are height independent (with $c_*=F_c/\rho u_*$). This seems theoretically incorrect statement and need justification.

Response: The notation H(z) and E(z) in these equations is for consistency because the equations apply both above and within the canopy. For clarification, we added the sentence: "*Fluxes above the canopy are obtained from MOST flux–gradient relationships as modified for the RSL, and K_c within the canopy is obtained from the momentum and scalar balance equations for plant canopies (section 2.2).*"

page 9, line 184: The scalar diffusivity (K_c) is assumed to be the same for heat and water vapor. It has to be shown that this is not always the case, especially near the canopy top (e.g. please see Shapkalijevski et al. 2016, Fig. 1).

Response: We revised this to read: "…with K_c the scalar diffusivity ($m^2\ s^{-1}$), assumed to be the same for heat and water vapor *as is common in land surface models though there are exceptions (e.g., Shapkalijevski et al. 2016)*.

page 12, line 242: '... additional source fluxes', but during day, and sink during night?

Response: We changed "source fluxes" to "*source/sink fluxes*". For consistency, we made the same change to "source flux" throughout the manuscript or deleted "source" as appropriate.

page 17, line 348-349 similar to the comment above on page 9, line 184.

Response: See our response to the previous comment.

page 18, line 366 Eq. 27, the roughness length for momentum and scalars are defined as invariant (fixed values), but no reference is given based on what. The RSL theory (Harman and Finnigan 2007; 2008) defines them as variant quantities, dependent on the flow/stratification and canopy properties. Further justification here would be very appreciated

Response: The roughness lengths used in Eq. 27 are for the ground surface under the canopy. There are taken from the CLM4.5. We added this reference to the text: "…roughness lengths of the ground for momentum and scalars, respectively, *as in the CLM4.5*…"

page 26, line 538: The wind speed, as simulated including the RSL effects in the flux-gradient relationship of momentum has smaller magnitude compared to the wind speed from the standard MOST. Looking at the profilles provided by Harman and Finnigan (2007), the wind profiles calculated by RSL is generally stronger compared to the wind profiles calculated by MOST. Any comment in the discussion about this would be also very appreciated.

Response: The reason for this is that the MOST profiles are calculated using prescribed roughness length and displacement height as in CLM4.5. We note this in the figure caption. The differences in roughness length and displacement height between MOST and RSL change both the value of u(z)/u* at the reference height and also the form of u(z).

page 28, line 579 The RSL effects are expected to have larger influence on nocturnal turbulent exchange (as assumed by the theory), due to shear-driven (canopy induced in this case) turbulence dominating

over the night (compared to thermal convection during day). This is excellent example that corroborates this assumption.

Response: We expanded upon this statement as suggested by the reviewer: "…primarily by increasing u_* at night *as expected due to shear-driven turbulence induced by the canopy dominating during night compared with day*."

page 32, line 666-672 Shapkalijevski et al. (2016) used the RSL theory (Harman and Finnigan 2007; 2008) over a canopy with different sparsity/density and explicitly calculated the β and the l_m/β scale as function of stability.

Response: We added this reference in the introduction: "… *observations above a walnut orchard further support the theory (Shapkalijevski et al. 2016).*"

page 66, Figure 1 It could be convenient for the readers if the displacement height and the roughness length are define in the schematic figure.

Response: We added to the figure caption: "*In the CLM4.5,* d *and* z_0 *are prescribed fractions of canopy height.*"

RC2

We thank the reviewer for their careful reading of the manuscript and attention to detail. These comments, and our responses as described below, improved the focus, clarity, and main points of the manuscript.

General comments

a. The pedigree of the model being tested is not fully clear, neither is its exact link with CLM4.5. Given the scope of the journal, as well as the importance of a widely used LSM like CLM, it is important to make this crystal clear.

Response: We revised section 2 (Methods) to better clarify the development of the multilayer model and its relation to CLM4.5. First, we split the section into two sections with: "*2 Model description*" and "*3 Model evaluation*". See also our response to detailed comments (10). Second, we revised the first paragraph in the model description to better give the history of the multilayer model and its capability. We show the current model is a further development of the previous work of Bonan et al. (2014). Specifically: "*Here, we describe the formulation of the scalar profiles and the RSL, which were not included in Bonan et al. (2014) and which replace the bulk canopy airspace parameterization.*"

The relationship to ORCHIDEE-CAN (also raised in detailed comments 3) is that we use a similar implicit coupling of the flux-profile equations and numerical solution. We acknowledge their work and point out differences with our own implementation. We revised the text to read: "The implementation is conceptually similar to the implementation of a multi-layer canopy in ORCHIDEE-CAN and that model's implicit numerical coupling of leaf fluxes and scalar profiles (Ryder et al., 2016; Chen et al., 2016). *That numerical scheme is modified here to include sunlit and shaded leaves at each layer in the canopy and also the RSL (Harman and Finnigan 2007, 2008). Whereas ORCHIDEE-CAN uses an implicit calculation of longwave radiative transfer for the leaf energy balance, we retain the Norman (1979) radiative transfer used by Bonan et al. (2014).*"

The relationship to CLM4.5 (also mentioned in detailed comments 3 and 8) is two-fold. First, we clarified the intent of the model simulations. In section 3.2 Model simulations we added: "*The CLM4.5 and the multi-layer canopy differ in several ways (Table 3). To facilitate comparison and to isolate specific model differences, we devised a series of simulations to incrementally test parameterizations changes (Table 4).*" Second, the manuscript is a "Development and technical paper" not a "Model description paper". We are describing a canopy parameterization that can be included in CLM4.5, not a specific version of CLM. We previously mentioned this in the code availability section. We also added a statement in the conclusion: "While this is an advancement over the CLM4.5, much work remains to fully develop this class of model *and to implement the multi-layer canopy parameterization in the CLM*."

b. Whereas part of the model uses vertically varying plant area densities, the model that describes the in-canopy turbulence profiles and wind profiles assumes a constant plant area density. This inconsistency seems to remain undiscussed.

Response: We added a sentence to our discussion of advantages and limitations in the model: "*The canopy length scale L_c is assumed to be constant with height as in Eq. (56) and is thought to be more conservative than either leaf area density or the leaf drag coefficient separately (Harman and Finnigan (2007). Massman (1997) developed a first-order closure canopy turbulence parameterization that accounts for vertical variation in leaf area density, but that is not considered here.*"

c. Figure 7-10 are to me the core of the analysis, showing how the different model modifications change the skill of the LSM. However, I wonder if the statistic used (RMSE, probably not bias-corrected) is the most informative measure to illustrate and understand the changes in model skill.

Response: We used RMSE because it is the most easily interpreted metric of model performance and improvement by sequentially adding new parameterizations. It is not biased corrected and simply assesses the summed error between the model and observations. We also looked at the Taylor skill score as a metric of model performance. It gives a similar assessment of the individual parameterization changes, but the reviewer noted in detailed comment (14) the difficulty in interpreting differences in model skill scores.

d. Although this is primarily a model-description paper, it does contain a clear research part (which I very much appreciate). However, it would then have been helpful to include a research question that matches the performed research (e.g. 'which of the model modifications had the most important positive impact on model performance for which model output, and for which sites'). Having such a research question would also make the conclusion more concrete.

Response: We added to the last paragraph of the introduction: "*The previous model development of Bonan et al. (2014) included improvements to stomatal conductance and canopy physiology compared with the CLM4.5. We contrast those developments with the RSL parameterization described herein and compare tall forest with short herbaceous vegetation to ascertain which aspects of the multi-layer canopy most improve the model.*"

e. (partly linked to the previous point) The paper misses a clear synthesis of the model evaluation results: what are the major tendencies with respect to skill: for what type of sites does which type of model improvement (multilayer, plant-physiology or RSL) have an impact on what type of model output. With that synthesis potential users of the model would directly know if the new model would have an important impact on their simulations.

Response: The biggest difference we see between sites relates to forest versus herbaceous. The plant physiological improvements occur across sites, but the RSL improvements most consistently occur at forest sites. We revised the abstract to read:

"*Advances in modeling stomatal conductance and canopy physiology beyond what is in the CLM4.5 substantially improve model performance at the forest sites. The signature of the roughness sublayer is most evident in nighttime friction velocity and the diurnal cycle of radiative temperature, but is also seen in sensible heat flux.*"

and:

"*The herbaceous sites also show model improvements, but the improvements are related less systematically to the roughness sublayer parameterization in these canopies.*"

Detailed comments

1. 72: in modelling (as opposed to observational studies) the issue is not so much that the flux is larger than inferred from the vertical gradient or difference, but rather the other way around. The lower boundary condition rather acts as a flux boundary condition (at least for daytime conditions) and hence the failure of MOST in describing the flow in the RSL leads to an *overestimation of the vertical differences* (for stable conditions this may be different as the nature of the boundary condition depends on the stability).

Response: We changed the wording to "… within the RSL *flux–profile relationships differ from MOST.*"

2. 75/76: similar remarks as remark 1 hold here: wind speed determines the *link* between temperature/concentration difference and the corresponding flux: it is not necessarily so that the flux is the *dependent variable* as the formulation may suggest.

Response: Our intent with this sentence is to show that land surface models must parameterize within-canopy turbulent processes in some manner. We changed the text to read: "*Dual-source land surface models also require parameterization of turbulent processes within the canopy. Following BATS (Dickinson et al., 1986), the CLM4.5 uses an ad-hoc parameterization without explicitly representing turbulence.*"

3. 84-86: the model on which the model that is tested in this paper is based is clearly identified with a reference. However, the relationship of that model to ORCHIDEE and to CLM4.5 is unclear. Please add a clear sketch of the origin of the currently used model, and its relationship to other models mentioned.

Response: The particular reference to ORCHIDEE here is merely to acknowledge the previous work of the ORCHIDEE group to develop a multi-layer version of their model (also published in GMD). The specific lineage of that to our work is discussed later. See our response to general comments (a).

4. 94-98: what I miss in the motivation is that with changing profiles of temperature, humidity and wind in the canopy, plant-related processed may also change. Since quite a large part of the simulations in the sensitivity analysis are devoted to those aspects it would be worthwhile to make this link in the introduction.

Response: We added to the introduction: "*We show that the resulting within-canopy profiles of temperature, humidity, and wind speed are a crucial aspect of the leaf to canopy flux scaling.*"

5. 108: the validation variables are clearly indicated (although I miss an indication of the temporal resolution used: hourly?), but the variables used to force the model are not indicated.

Response: The resolution is 30 minutes or 60 minutes depending on tower site. We added the sentence: "*The tower forcing and fluxes have a resolution of 30 minutes except for four sites (US-Ha1, US-MMS, US-UMB, US-Ne3) with 60 minute resolution.*" We also added text for the forcing variables: "*downwelling solar and longwave radiation, air temperature, relative humidity, wind speed, surface pressure, precipitation, and tower height*".

6. 113: I do not see why within a single month soil moisture variations would not need to be accounted for? Is this a rain-free month for each site, is there no dry-down happening? Do I have to interpret this remark as that soil moisture stress of the vegetation is assumed to be absent?

Response: We want to evaluate the canopy physics parameterizations in a clean manner without confounding effects from large changes in soil moisture. We revised the sentence to read: "… *so as to evaluate the canopy physics parameterizations without confounding effects of seasonal changes in soil water*."

7. 114-130: the enumeration of site parameters seems to be somewhat random (for different sites, different parameters are mentioned). I would suggest to extend the table to include the site-dependent parameters, and to add a reference (as a table footnote) for each site.

Response: The text in these two paragraphs (now moved to *section 3.1 Flux tower data*) describes how we obtained vegetation data for the new sites not previously described in Bonan et al. (2014). This includes the type of crop (for the agricultural sites), canopy height, and leaf area index. These variables are provided in Table 2, and the text here documents how those values were obtained. Also, we provide documentation for the tower data.

8. 144: here CLM4.5 surfaces: if I understand it well (see also remark 3) the multilayer model is constructed in such a way that a number of parameterizations are close to what is used in CLM4.5 so that a comparison between CLM4.5 and the simplest version of the multilayer model would – approximately- only test the transition from single layer to multi-layer. As per remark 3: please clarify the strategy.

Response: See our response to general comments (a).

9. 152: Figure 1: for the reader to appreciate the sensitivities of modelled fluxes to the different step changes in the parameterizations later on, it would perhaps be helpful to sketch a more conceptual picture that shows which variables and which resistances are affected by which part of the model improvements: the multi-layer coupling, the plant-related parameterizations or the turbulence-related (RSL) parameterizations. If not in a separate figure it could perhaps be implemented by using three different colors in Figure 1 to identify which parts are directly affected by which part of the model improvement.

Response: The intent of Figure 1 is to show readers the numerical grid used in the multilayer canopy and contrast this representation with the dual source canopy used in the CLM4.5. Table 3 specifically describes parameterization differences between the multilayer canopy and the CLM4.5.

10. Section 2.1.1: for easier reference it would be helpful to introduce an extra level of sectioning: users of your model will more easily be able to find the aspect they need (e.g. (1) canopy-space scalar budget, (2) leave energy balance, (3) vertical discretization, (4) numerical solution). Since this would make the section numbers excessively long, you could consider to make the model description, which in the end is the main reason for this paper, a separate chapter, rather than section 2.1 (2. Model formulation, 3 Data and methods).

Response: We split section 2 (Methods) into two separate sections: *2 Model description* and *3 Model evaluation*. The multilayer canopy has two main components: (1) the canopy flux-profile equations and (2) the roughness sublayer parameterization. These are described in separate sub-sections of the model

description. Additional sub-sections describe leaf area density and leaf heat capacity. We note that section 2.1 (flux-profile equations) follows the sequence that the reviewer suggested.

11. 302: the derivation of the RSL-model also requires/implies a *vertically* homogeneous canopy (in terms of leaf area density). In principle this is at odds with the explicit use of vertically varying plant area densities (see section 2.1.3). The effect of this inconsistency seems to remain undiscussed.

Response: See our response to general comments (b).

12. Chapter 3 would also benefit from a division in subsections.

Response: We divided the results into three sub-sections: *4.1 Model evaluation*, *4.2 Effect of specific parameterizations*, and *4.3 Canopy profiles*

13. 477 and further (discussion of Table 5). For the interpretation of the results it is important to know what is roughly the partitioning between latent and sensible heat flux: this is an important factor in determining how sensitive fluxes are to changes in the aerodynamic resistance (both between leaf and canopy air, and between canopy and surface layer). The sensitivity to a certain change in aerodynamic resistance may even change sign, and for a given amount of available energy the sensitivities of sensible and latent heat flux are of opposite sign. If the energy partitioning is different between the sites, this might also explain some of the differences in the sensitivities observed in figures 7 to 10.

Response: We agree that this is a useful point, but it is beyond the scope of the manuscript. There is a rich literature considering the differences between aerodynamic and physiological controls of surface fluxes and when, for example, a change in stomatal resistance or aerodynamic resistance may or may not affect latent heat flux. The manuscript is already quite long, and to address this beyond a cursory manner would require substantial text and figures. We prefer that the manuscript remain focused on our intent: that the CLM4.5 canopy parameterization is flawed, and that a multilayer canopy model with improved leaf biophysics and turbulence improves upon the CLM4.5.

14. 478: In the interpretation of the results in Table 5 it would be helpful to have an indication as to how significant the change in skill of the new model is, compared to CLM4.5. Some changes are very clear, others seem to be marginal (in both directions). I would suggest to limit the discussion to the significant ones.

Response: We use Table 5 as a summary to assess whether the model is, overall across many sites, performing better than CLM4.5. We then use Figures 4, 5, and 6 as detailed flux evaluations for specific sites. Figures 7-10 address why the model is performing better. We agree that the interpretation of the Taylor skill score is not necessarily intuitive (how much better is 0.94 vs. 0.92; US-Ha1 latent heat flux). Nonetheless, the skill score is a composite measure of the data points on a Taylor plot such as Figure 5. The average skill scores presented in Table 5 are exactly what the reviewer requested in comment (20) below.

15. 499: 'complex': I would say that this type of behavior is well-known: for moderate cooling the turbulence is sustained and a more or less monotonous relationship between sensible heat flux exists. However, when the cooling exceeds a certain limit (or wind speed drops below a certain limit) turbulence vanishes and the relationship between temperature difference (finite) and heat flux (tends to zero) is lost (check literature on 'maximum sustainable heat flux'). In that case the surface

temperature is the result of the interplay between radiative cooling, supply of heat flow below (soil of lower canopy) and some remaining weak turbulence that supplies heat from above. It would be interesting to know which of the steps from CLM4.5 to ML+RSL makes the change in realism here (which, by the way, is a very relevant result).

Response: The functional relationship between H and ΔT is an important way to test the model in addition to direct comparison between observed and modeled fluxes such as presented in Figure 4. The main point here is that CLM4.5 shows a very different pattern compared to the observations (for the forest sites) and that the new canopy model better matches the observations. We revised the figure to include the ML-RSL simulation so that we can clearly distinguish the influence of the RSL. We added a sentence to the results section: "*The primary effect of the RSL is to reduce high daytime temperatures and to increase sensible heat transfer to the surface at night*"; and to the discussion of Figure 6: "*Additional improvement, as expected from the RSL theory, is seen during moderately stable periods, which in turn reduces surface cooling.*"

16. 565: if the results are degraded by the inclusion of the RSL description, then apparently the change in flux that resulted from the updated biophysics was too large? Or could there be another reason for this degradation?

Response: The main point here is that the RSL parameterization cannot be evaluated independent of changes in leaf biophysics. We return to this point later in the conclusions.

17. 573-574: I do not see why the question whether the observations were made inside or above the RSL would matter here. The relationship between ASL-temperature and canopy temperature is just different between RSL-enabled models and pure MOST. For high canopies the ASL observation is closer (in terms of multiples of RSL height) to the canopy than for low canopies. Hence for high canopies the difference between RSL-estimates of the canopy temperature and MOST-estimate is large as compared to the total vertical temperature difference. On the other hand, for low canopies the largest part of the vertical temperature difference occurs above the RSL (in which MOST is supposed to be valid), hence the error in the within-RSL profile has little weight in the total vertical temperature difference.

Response: We deleted the phrase "because the measurements were taken above the RSL."

18. 701-702: what are these minimum values for the conductances?

Response: The maximum resistance is 500 s/m. See our discussion of Eqs. 24-27, which describe the conductances.

19. Figure 4: is the RMSE reported in the figures bias-corrected or does it include the RMSE due to the bias?

Response: The RMSE is not bias corrected. See our response to general comment (c).

20. Figure 5: I wonder why the different years are shown as separate symbols. I would be more interested in seeing all sites plotted in the same figure (with a single symbol giving the multi-year statistics) so that we can try to understand to what extent the different sites show different skills as can be seen in table 5).

Response: Table 5 conveys the information on model performance at each site (averaged across years) that the reviewer requests. Figure 4 then provides a detailed analysis of the diurnal cycle at one site for one year (US-UMB) and Figure 5 provides an analysis of all years at that site.

21. Figure 6: although these figures are very informative, and show a clear change between the different model versions, it is unclear why the points in these figures should be well behaved. The link between temperature difference and heat flux is indirect: friction velocity and stability are variables that enter into this relationship (or wind speed and stability if one would use a drag-law formulation).

Response: See comment (15) above.

22. Figure 7-10: is the RMSE shown here bias-corrected? If not, it is not full clear whether we look at biases (interesting in themselves, but then show biases in the graphs) or a mix of mean bias and incorrect dynamics.

Response: The RMSE is not bias corrected. See our response to general comment (c).

Very detailed comments

1. 87: 'this class' refers to RSL-aware models, or multi-layer models?

Response: We changed "this class of canopy models" to "*multilayer models*".

2. 106: in Table 1 mean annual temperature and annual (?) precipitation are given. To understand the climatological setting this is OK, but to understand the data that we will be looking at values representative for July might perhaps be more informative.

Response: We updated the table to provide values for the particular month.

3. 151-152: if no scalar profiles included in Bonan et al. (2014), then how did the plant-related processes obtain information on in-canopy temperature and humidity?

Response: The model of Bonan et al. (2014) used a bulk canopy air space parameterization. We added text to state this: "*Temperature, humidity, and wind speed in the canopy are calculated using a bulk canopy airspace.*" We also added text to explain that the new model replaces the bulk canopy airspace: "Here, we describe the formulation of the scalar profiles and the RSL, which were not included in Bonan et al. (2014) *and which replace the bulk canopy airspace parameterization*."

4. 152: 'The approach': does this refer to the grid?

Response: We changed "approach" to "*implementation*".

5. 170: 'vertical flux H': in fact it should be the vertical divergence of the vertical flux that affects the temperature.

Response: We changed this to read vertical flux divergence of H. We made the same change for E in the next equation.

6. 179: as in Harman and Finnigan (2007, 2008): it would be useful to refer forward to the location where the parameterization of the turbulent diffusivities is described in this paper.

Response: We modified the text to refer to section 2.2, where this is discussed.

7. 202-203: you indicate that a conductance is needed for evapotranspiration from partially wetted leaves: please refer forward to equation 12 to reassure the reader that you will take care of this.

Response: We modified the text to refer to equation 12.

8. 214-215: 'The next three terms ...': in fact these three terms describe the flux *divergence*.

Response: Corrected.

9. 216-217: please refer forward to section 2.1.2 to the description the aerodynamic conductance.

Response: We added text to refer to equations 24 and 26.

10. 316: also interpret l_m as the mixing length in the canopy. This interpretation now occurs only at line 324.

Response: We are specifically referring to l_m/β not l_m. We clarified this by changing "This length scale is…" to "The length scale l_m/β is…"

11. 467: is the modelled upward longwave flux solely determined by the temperature of the upper canopy layer or does the layer below the top also contribute? Not much is said about how radiative transfer is handled (except for the references in line 139).

Response: Longwave radiation is treated in a multilayer framework so that all layers contribute to the upward flux above the canopy. We refer the reviewer (and readers of the manuscript) to the Norman (1979) paper that we cite.

12. 493: this is a rather long sentence: do you intend to say that these sites where selected because they had a small RMS for sensible heat flux and surface temperature?

Response: Yes. We broke the sentence into two parts and explained that the sites were selected because they have small RMSE: "*These sites were chosen because the root mean square error of the model (ML+RSL) is low for H and T_{rad}.*"

13. 498: 'data': do you mean simulation results or observations?

Response: We changed "data" to "*CLM4.5 data*".

14. 609-613: check this sentence (long, multiple messages, broken?)

Response: We broke this into separate sentences: "*The importance of within-canopy temperature gradients is seen in forest canopies. The microclimatic influence of dense forest canopies buffers the impact of macroclimatic warming on understory plants (De Frenne et al., 2013), and the vertical climatic gradients in tropical rainforests are steeper than elevation or latitudinal gradients (Scheffers et al., 2013).*"

15. Figure 7, line 1225: it is not fully clear what is shown here. I interpret the bar graphs as showing the percentage *change* in RMSE relative to CLM4.5. Then a large negative value would be optimal (-100 would be perfect). In that sense the metric is a bit confusing since showing a mix of positive and negative values might suggest a bias plot to the reader, rather than an RMSE(-change) plot.

Response: The reviewer is correct in their interpretation of the bar graphs. We are showing the reduction in RMSE relative to CLM4.5. We added text to the figure caption: "*A negative value shows a reduction in RMSE relative to CLM4.5 and indicates model improvement.*"

Modeling canopy-induced turbulence in the Earth system: a unified parameterization of turbulent exchange within plant canopies and the roughness sublayer (CLM-ml v0)

Gordon B. Bonan[1]
Edward G. Patton[1]
Ian N. Harman[2]
Keith W. Oleson[1]
John J. Finnigan[2]
Yaqiong Lu[1]
Elizabeth A. Burakowski[3]

1 National Center for Atmospheric Research, P. O. Box 3000, Boulder, Colorado, USA 80307
2 CSIRO Oceans and Atmosphere, Canberra, Australia
3 University of New Hampshire, Durham, New Hampshire, USA

Corresponding author: G. B. Bonan (bonan@ucar.edu)

Abstract. Land surface models used in climate models neglect the roughness sublayer and parameterize within-canopy turbulence in an ad hoc manner. We implemented a roughness sublayer turbulence parameterization in a multi-layer canopy model (CLM-ml v0) to test if this theory provides a tractable parameterization extending from the ground through the canopy and the roughness sublayer. We compared the canopy model with the Community Land Model (CLM4.5) at 7 forest, 2 grassland, and 3 cropland AmeriFlux sites over a range of canopy height, leaf area index, and climate. The CLM4.5 has pronounced biases during summer months at forest sites in mid-day latent heat flux, sensible heat flux, and gross primary production, nighttime friction velocity, and the radiative temperature diurnal range. The new canopy model reduces these biases by introducing new physics. Advances in modeling stomatal conductance and canopy physiology beyond what is in the CLM4.5 substantially improve model performance at the forest sites. The signature of the roughness sublayer is most evident in nighttime friction velocity and the diurnal cycle of radiative temperature, but is also seen in sensible heat flux. Within-canopy temperature profiles are markedly different compared with profiles obtained using Monin–Obukhov similarity theory, and the roughness sublayer produces cooler daytime and warmer nighttime temperatures. The herbaceous sites also show model improvements, but the improvements are related less systematically to the roughness sublayer parameterization in these canopies. The multi-layer canopy with the roughness sublayer turbulence improves simulations compared with the CLM4.5 while also advancing the theoretical basis for surface flux parameterizations.

Keywords: multi-layer canopy, roughness sublayer, Monin–Obukhov similarity theory, wind profile, scalar profile, land surface model

Deleted: sensible heat flux,

Deleted: short

1 Introduction

Distinct parameterizations of land surface processes, separate from the atmospheric physics, were coupled to global climate models in the mid-1980s with the Biosphere–Atmosphere Transfer Scheme (BATS; Dickinson et al., 1986) and the Simple Biosphere Model (SiB; Sellers et al., 1986). While carbon cycle feedbacks have since gained prominence in terms of model development and study of biotic feedbacks with climate change (Friedlingstein et al., 2006, 2014), the fundamental coupling between plants and the atmosphere in climate models still occurs with the fluxes of momentum, energy, and mass over the diurnal cycle as mediated by plant physiology, the microclimate of plant canopies, and boundary layer processes. The central paradigm of land surface models, as originally devised by Deardorff (1978) and carried forth with BATS, SiB, and subsequent models, has been to represent plant canopies as a homogeneous "big leaf" without vertical structure, though with separate fluxes for vegetation and soil. A critical advancement was to analytically integrate leaf physiological processes over profiles of light and nitrogen in the canopy (Sellers et al., 1996) and to extend the canopy to two big leaves to represent sunlit and shaded portions of the canopy (Wang and Leuning, 1998; Dai et al., 2004).

Deleted: source

In land surface models such as the Community Land Model (CLM4.5; Oleson et al., 2013), for example, fluxes of heat and moisture occur from the leaves to the canopy air, from the ground to the canopy air, and from the canopy air to the atmosphere (Figure 1a). The flux from the canopy to the atmosphere is parameterized using Monin–Obukhov similarity theory (MOST).

This theory requires the displacement height (d) and roughness length (z_0). A challenge has been to specify these, which are complex functions of the flow and physical canopy structure (Shaw and Pereira 1982); simple parameterizations calculate them as a fixed fraction of canopy height (as in the CLM4.5) or use relationships with leaf area index (Sellers et al., 1986; Choudhury and Monteith, 1988; Raupach, 1994). An additional challenge, largely ignored in land surface models, is that MOST fails in the roughness sublayer (RSL) extending to twice the canopy height or more (Garratt, 1978; Physick and Garratt, 1995; Harman and Finnigan, 2007, 2008). While MOST successfully relates mean gradients and turbulent fluxes in the surface layer above the RSL, within the RSL flux–profile relationships differ from MOST. Dual-source land surface models also require parameterization of turbulent processes within the canopy. Following BATS (Dickinson et al., 1986), the CLM4.5 uses an ad-hoc parameterization without explicitly representing turbulence. Wind speed within the canopy is taken as equal to the friction velocity (u_*), and the aerodynamic conductance between the ground and canopy air is proportional to u_*. Zeng et al. (2005) subsequently modified this expression to account for sparse and dense canopies.

Harman and Finnigan (2007, 2008) proposed a formulation by which traditional MOST can be modified to account for the RSL. Their theoretical derivations couple the above-canopy turbulent fluxes with equations for the mass and momentum balances within the canopy. They tested the theory with observations for eucalyptus and pine forests, and observations above a walnut orchard further support the theory (Shapkalijevski et al. 2016). Harman (2012) examined the consequences of the RSL in a bulk surface flux parameterization coupled to an atmospheric boundary layer model. Here, we implement and test the theory in a multi-layer canopy model (Bonan et al., 2014). The development of a multi-layer canopy for the ORCHIDEE land surface

Deleted: vertical fluxes are larger than expected from mean gradients obtained using

Deleted: , where wind speed regulates vegetation fluxes through the leaf boundary layer conductance and where turbulent transport regulates fluxes between the ground and canopy air

Deleted: without resolving within-canopy profiles of wind speed or turbulence

model has renewed interest in the practical use of multi-layer models (Ryder et al., 2016; Chen et al., 2016). The earlier multi-layer model development of Bonan et al. (2014) focused on linking stomatal conductance and plant hydraulics and neglected turbulent processes in the canopy. The current work extends the model to include canopy-induced turbulence. The RSL theory avoids a priori specification of z_0 and d by linking these to canopy density and characteristics of the flow; provides consistent forms for various turbulent terms above and within the canopy (friction velocity, wind speed, scalar transfer coefficients); and provides a method for determining the associated profiles of air temperature and water vapor concentration within the canopy.

Deleted: this class of canopy

Deleted: canopy

This study is motivated by the premise that land surface models generally neglect canopy-induced turbulence, that inclusion of this is critical to model simulations, and that the Harman and Finnigan (2007, 2008) RSL theory provides a tractable parameterization extending from the ground through the canopy and the RSL. We show that the resulting within-canopy profiles of temperature, humidity, and wind speed are a crucial aspect of the leaf to canopy flux scaling. The previous model development of Bonan et al. (2014) included improvements to stomatal conductance and canopy physiology compared with the CLM4.5. We contrast those developments with the RSL parameterization described herein and compare tall forest with short herbaceous vegetation to ascertain which aspects of the multi-layer canopy most improve the model.

2 Model description

The canopy model has three main components: leaf gas exchange and plant hydraulics; a numerical solution for scalar profiles within and above the canopy; and inclusion of the RSL parameterization. It builds upon the work of Bonan et al. (2014), which describes leaf gas

exchange and plant hydraulics for a multi-layer canopy with sunlit and shaded leaves at each layer in the canopy. The calculation of leaf temperature and fluxes is solved simultaneously with stomatal conductance, photosynthesis, and leaf water potential in an iterative calculation. This method numerically optimizes water-use efficiency within the constraints imposed by plant water uptake to prevent leaf desiccation using the methodology of Williams et al. (1996). Radiative transfer of visible, near-infrared, and longwave radiation is calculated at each level and accounts for forward and backward scattering within the canopy. Bonan et al. (2014) used the radiative transfer model of Norman (1979). We retain that parameterization for longwave radiation, but radiative transfer in the visible and near-infrared wavebands is calculated from the two-stream approximation with the absorbed solar radiation partitioned into direct beam, scattered direct beam, and diffuse radiation for sunlit and shaded leaves in relation to cumulative plant area index as in Dai et al. (2004). This allows better comparison with the CLM4.5, which uses the canopy-integrated two-stream solution for sunlit and shaded leaves. Soil fluxes are calculated using the layer of canopy air immediately above the ground. Temperature, humidity, and wind speed in the canopy are calculated using a bulk canopy airspace. Bonan et al. (2014) provide further details.

Here, we describe the formulation of the scalar profiles and the RSL, which were not included in Bonan et al. (2014) and which replace the bulk canopy airspace parameterization. Figure 1 shows the numerical grid. The implementation is conceptually similar to the multi-layer canopy in ORCHIDEE-CAN and that model's implicit numerical coupling of leaf fluxes and scalar profiles (Ryder et al., 2016; Chen et al., 2016). That numerical scheme is modified here to include sunlit and shaded leaves at each layer in the canopy and also the RSL (Harman and Finnigan 2007, 2008). Whereas ORCHIDEE-CAN uses an implicit calculation of longwave

Deleted: The calculation of leaf temperature and fluxes is solved simultaneously with stomatal conductance, photosynthesis, and leaf water potential in an iterative calculation. This method numerically optimizes water-use efficiency within the constraints imposed by plant water uptake to prevent leaf desiccation using the methodology of Williams et al. (1996).

Deleted: approach

Deleted: implementation of a

Deleted: , but modified

radiative transfer for the leaf energy balance, we retain the Norman (1979) radiative transfer used by Bonan et al. (2014). The grid spacing (Δz) is 0.5 m for forest and 0.1 m for crop and grassland. We use thin layers to represent the light gradients that drive variation in leaf water potential in the canopy as in Bonan et al. (2014). Indeed, it is this strong variation in leaf water potential from the top of the canopy to the bottom that motivates the need for a multi-layer canopy. Appendix A provides a complete description of the canopy model, and Appendix B lists all model variables.

2.1 The coupled flux–profile equations

In the volume of air extending from the ground to some reference height above the canopy, the scalar conservation equations for heat and water vapor, the energy balances of the sunlit and shaded canopy, and the ground energy balance provide a system of equations that can be solved for air temperature, water vapor concentration, sunlit and shaded leaf temperatures, and ground temperature. The scalar conservation equation for heat relates the change over some time interval of air temperature (θ, K) at height z (m) to the source/sink fluxes of sensible heat from the sunlit and shaded portions of the canopy ($H_{\ell sun}$ and $H_{\ell sha}$, W m^{-2}) and the vertical flux divergence ($\partial H / \partial z$, W m^{-3}). For a vertically-resolved canopy, the one-dimensional conservation equation for temperature is

$$\rho_m c_p \frac{\partial \theta(z)}{\partial t} + \frac{\partial H}{\partial z} = \left[H_{\ell sun}(z) f_{sun}(z) + H_{\ell sha}(z) \{1 - f_{sun}(z)\} \right] a(z) \quad (1)$$

The equivalent equation for water vapor (q, mol mol^{-1}) in relation to the canopy source/sink fluxes ($E_{\ell sun}$ and $E_{\ell sha}$, mol H_2O m^{-2} s^{-1}) and vertical flux divergence ($\partial E / \partial z$, mol H_2O m^{-3} s^{-1}) is

$$\rho_m \frac{\partial q(z)}{\partial t} + \frac{\partial E}{\partial z} = \left[E_{\ell sun}(z) f_{sun}(z) + E_{\ell sha}(z) \{1 - f_{sun}(z)\} \right] a(z) \quad (2)$$

In this notation, ρ_m is molar density (mol m^{-3}) and c_p is the specific heat of air (J mol^{-1} K^{-1}). $a(z)$ is the plant area density, which is equal to the leaf and stem area increment of a canopy layer divided by the thickness of the layer ($\Delta L(z) / \Delta z$; m^2 m^{-3}), and f_{sun} is the sunlit fraction of the layer. As in Harman and Finnigan (2007, 2008), the vertical fluxes are parameterized using a first-order turbulence closure (K-theory) whereby the sensible heat flux is

$$H(z) = -\rho_m c_p K_c(z) \frac{\partial \theta}{\partial z} \quad (3)$$

and the water vapor flux is

$$E(z) = -\rho_m K_c(z) \frac{\partial q}{\partial z} \quad (4)$$

with K_c the scalar diffusivity (m^2 s^{-1}), assumed to be the same for heat and water vapor as is common in land surface models though there are exceptions (e.g., Shapkalijevski et al. 2016). These equations apply above and within the canopy, but with $a(z) = 0$ for layers without vegetation. Fluxes above the canopy are obtained from MOST flux–gradient relationships as modified for the RSL, and K_c within the canopy is obtained from the momentum and scalar balance equations for plant canopies (section 2.2).

The source/sink fluxes of sensible heat and water vapor are described by the energy balance equation and are provided separately for sunlit and shaded fractions of the canopy layer. The energy balance of sunlit leaves at height z in the canopy is

$$c_L(z) \frac{\partial T_{\ell sun}(z)}{\partial t} \Delta L_{sun}(z) = \left[R_{n\ell sun}(z) - H_{\ell sun}(z) - \lambda E_{\ell sun}(z) \right] \Delta L_{sun}(z) \quad (5)$$

The left-hand side is the storage of heat (W m^{-2}) in a layer of vegetation with heat capacity c_L (J m^{-2} K^{-1}), temperature $T_{\ell sun}$ (K), and plant area index $\Delta L_{sun} = f_{sun}\Delta L$ (m^2 m^{-2}). The right-hand side is the balance between net radiation ($R_{n\ell sun}$; positive denotes energy gain), sensible heat flux ($H_{\ell sun}$; positive away from the leaf), and latent heat flux ($\lambda E_{\ell sun}$; positive away from the leaf). The sensible heat flux is

$$H_{\ell sun}(z) = 2c_p\left[T_{\ell sun}(z) - \theta(z)\right]g_b(z) \tag{6}$$

and the evapotranspiration flux is

$$E_{\ell sun}(z) = \left[q_{sat}\left(T_{\ell sun}\right) - q(z)\right]g_{\ell sun}(z) \tag{7}$$

For sensible heat, g_b is the leaf boundary layer conductance (mol m^{-2} s^{-1}), and the factor two appears because heat transfer occurs from both sides of plant material. The evapotranspiration flux depends on the saturated water vapor concentration of the leaf, which varies with leaf temperature and is denoted as $q_{sat}(T_{\ell sun})$. It also requires a leaf conductance ($g_{\ell sun}$, mol m^{-2} s^{-1}) that combines evaporation from the wetted fraction of the canopy and transpiration from the dry fraction, as described by Eq. (12). A similar equation applies to shaded leaves. The energy balance given by Eq. (5) does not account for snow in the canopy, so the simulations are restricted to snow-free periods.

These equations are discretized in space and time and are solved in an implicit system of equations for time $n+1$. Ryder et al. (2016) and Chen et al. (2016) describe the solution using a single leaf. Here, the solution is given for separate sunlit and shaded portions of the canopy. In numerical form and with reference to Figure 1, the scalar conservation equation for temperature is

$$\frac{\rho_m \Delta z_i}{\Delta t} c_p \left(\theta_i^{n+1} - \theta_i^n\right) - g_{a,i-1} c_p \theta_{i-1}^{n+1} + \left(g_{a,i-1} + g_{a,i}\right) c_p \theta_i^{n+1} - g_{a,i} c_p \theta_{i+1}^{n+1} = 2 g_{b,i} c_p \left(T_{\ell sun,i}^{n+1} - \theta_i^{n+1}\right) \Delta L_{sun,i} + 2 g_{b,i} c_p \left(T_{\ell sha,i}^{n+1} - \theta_i^{n+1}\right) \Delta L_{sha,i} \quad (8)$$

and for water vapor is

$$\frac{\rho_m \Delta z_i}{\Delta t} \left(q_i^{n+1} - q_i^n\right) - g_{a,i-1} q_{i-1}^{n+1} + \left(g_{a,i-1} + g_{a,i}\right) q_i^{n+1} - g_{a,i} q_{i+1}^{n+1} = \left[q_{sat}\left(T_{\ell sun,i}^n\right) + s_i^{sun}\left(T_{\ell sun,i}^{n+1} - T_{\ell sun,i}^n\right) - q_i^{n+1}\right] g_{\ell sun,i} \Delta L_{sun,i} + \left[q_{sat}\left(T_{\ell sha,i}^n\right) + s_i^{sha}\left(T_{\ell sha,i}^{n+1} - T_{\ell sha,i}^n\right) - q_i^{n+1}\right] g_{\ell sha,i} \Delta L_{sha,i} \quad (9)$$

The first term on the left-hand side of Eq. (8) is the storage of heat (W m^{-2}) over the time interval Δt (s) in a layer of air with thickness Δz_i (m). The next three terms describe the vertical flux divergence from Eq. (3). These use conductance notation in which g_a is an aerodynamic conductance (mol m^{-2} s^{-1}), as described Eqs. 24 and 26. $g_{a,i}$ is the aerodynamic conductance between layer i to $i+1$ above, and $g_{a,i-1}$ is the similar conductance below between layer i to $i-1$. The two terms on the right-hand side of Eq. (8) are the vegetation source/sink fluxes of sensible heat for the sunlit and shaded portions of the canopy layer. Eq. (9) uses comparable terms for water vapor, with $q_{sat}(T_{\ell sun})$ and $q_{sat}(T_{\ell sha})$ linearized as explained below.

The sunlit and shaded temperatures required for Eqs. (8) and (9) are obtained from the energy balance at canopy layer i. For the sunlit portion of the canopy

$$\frac{c_{L,i}}{\Delta t}\left(T_{\ell sun,i}^{n+1} - T_{\ell sun,i}^n\right) = R_{n\ell sun,i} - 2 g_{b,i} c_p \left(T_{\ell sun,i}^{n+1} - \theta_i^{n+1}\right) - \lambda\left[q_{sat}\left(T_{\ell sun,i}^n\right) + s_i^{sun}\left(T_{\ell sun,i}^{n+1} - T_{\ell sun,i}^n\right) - q_i^{n+1}\right] g_{\ell sun,i} \quad (10)$$

Latent heat flux uses the linear approximation

$$q_{sat}\left(T_{\ell sun,i}^{n+1}\right) = q_{sat}\left(T_{\ell sun,i}^n\right) + s_i^{sun}\left(T_{\ell sun,i}^{n+1} - T_{\ell sun,i}^n\right) \quad (11)$$

Deleted: es

Deleted: that is nominally related to $\rho_m K_c / \Delta z$ (Eq. (25) provides the formal relationship)

with $s_i^{sun} = dq_{sat} / dT$ evaluated at $T_{\ell sun,i}^n$. The leaf boundary layer conductance ($g_{b,i}$) depends on wind speed (u_i, m s^{-1}) as described by Bonan et al. (2014). The conductance for transpiration is equal to the leaf boundary layer and stomatal conductances acting in series, i.e., $(g_{b,i}^{-1} + g_{sun,i}^{-1})^{-1}$. Here, it is assumed that $g_{b,i}$ is the same for heat and water vapor (as in the CLM4.5). Stomatal conductance ($g_{sun,i}$) is calculated based on water-use efficiency optimization and plant hydraulics (Bonan et al., 2014). The total conductance ($g_{\ell sun,i}$) combines evaporation from the wetted fraction of the plant material ($f_{wet,i}$) and transpiration from the dry fraction ($f_{dry,i}$), similar to that in the CLM4.5 in which

$$g_{\ell sun,i} = \left(\frac{g_{sun,i} g_{b,i}}{g_{sun,i} + g_{b,i}} \right) f_{dry,i} + g_{b,i} f_{wet,i} \tag{12}$$

with $f_{dry,i} = f_{green,i}(1 - f_{wet,i})$ so that interception occurs from stems and leaves, but transpiration occurs only from green leaves (denoted by the green leaf fraction $f_{green,i}$). The comparable equation for shaded leaves is

$$\begin{aligned} \frac{c_{L,i}}{\Delta t}\left(T_{\ell sha,i}^{n+1} - T_{\ell sha,i}^n\right) = {} & R_{n\ell sha,i} - 2c_p\left(T_{\ell sha,i}^{n+1} - \theta_i^{n+1}\right) g_{b,i} \\ & - \lambda\left[q_{sat}\left(T_{\ell sha,i}^n\right) + s_i^{sha}\left(T_{\ell sha,i}^{n+1} - T_{\ell sha,i}^n\right) - q_i^{n+1} \right] g_{\ell sha,i} \end{aligned} \tag{13}$$

We use post-CLM4.5 changes in intercepted water (W, kg m^{-2}) and the wet and dry fractions of the canopy (f_{wet}, f_{dry}) that are included in the next version of the model (CLM5).

At the lowest layer above the ground ($i = 1$), the ground fluxes H_0 and E_0 are additional source/sink fluxes, and the ground surface energy balance must be solved to provide the ground temperature (T_0^{n+1}, K). This energy balance is

$$R_{n0} = c_p\left(T_0^{n+1} - \theta_1^{n+1}\right) g_{a,0} + \lambda\left\{h_{s0}\left[q_{sat}\left(T_0^n\right) + s_0\left(T_0^{n+1} - T_0^n\right)\right] - q_1^{n+1}\right\} g_{s0} + \frac{\kappa_{soil}}{\Delta z_{soil}}\left(T_0^{n+1} - T_{soil}^n\right) \quad (14)$$

The first term on the right-hand side is the sensible heat flux between the ground with temperature T_0 and the air in the canopy layer immediately above the ground with temperature θ_1; $g_{a,0}$ is the corresponding aerodynamic conductance. The second term is the latent heat flux, with q_1 the water vapor concentration of the canopy air. In calculating soil evaporation, the surface water vapor concentration is

$$q_0^{n+1} = h_{s0} q_{sat}\left(T_0^{n+1}\right) = h_{s0}\left[q_{sat}\left(T_0^n\right) + s_0\left(T_0^{n+1} - T_0^n\right)\right] \quad (15)$$

with $s_0 = dq_{sat}/dT$ evaluated at T_0^n. Evaporation depends on the fractional humidity of the first soil layer (h_{s0}; CLM5). The soil evaporative conductance (g_{s0}) is the total conductance and consists of the aerodynamic conductance ($g_{a,0}$) and a soil surface conductance to evaporation (g_{soil}; CLM5) acting in series. The last term in Eq. (14) is the heat flux to the soil, which depends on the thermal conductivity (κ_{soil}), thickness (Δz_{soil}), and temperature (T_{soil}) of the first soil layer. Eq. (14) does not account for snow on the ground, and the simulations are restricted to snow-free periods.

The numerical solution involves rewriting Eqs. (10) and (13) to obtain expressions for $T_{\ell sun,i}^{n+1}$ and $T_{\ell sha,i}^{n+1}$ and substituting these in Eqs. (8) and (9). Eqs. (14) and (15) provide the necessary expressions for T_0^{n+1} and q_0^{n+1} at $i = 1$. This gives a tridiagonal system of implicit equations with the form

$$a_{1,i}\theta_{i-1}^{n+1} + b_{11,i}\theta_i^{n+1} + b_{12,i}q_i^{n+1} + c_{1,i}\theta_{i+1}^{n+1} = d_{1,i} \quad (16)$$

$$a_{2,i}q_{i-1}^{n+1} + b_{21,i}\theta_i^{n+1} + b_{22,i}q_i^{n+1} + c_{2,i}q_{i+1}^{n+1} = d_{2,i} \quad (17)$$

in which $a_{1,i}$, $a_{2,i}$, $b_{11,i}$, $b_{21,i}$, $b_{12,i}$, $b_{22,i}$, $c_{1,i}$, $c_{2,i}$, $d_{1,i}$, and $d_{2,i}$ are algebraic coefficients (Appendix A1). The system of equations is solved using the method of Richtmyer and Morton (1967, pp. 275–278), as described in Sect. S1 of the Supplement. θ_i^{n+1} and q_i^{n+1} are obtained for each level with the boundary conditions θ_{ref}^{n+1} and q_{ref}^{n+1} the temperature and water vapor concentration at some reference height above the canopy. Then, the leaf temperatures and fluxes and ground temperature and fluxes are evaluated. Ryder et al. (2016) used a different, but algebraically equivalent, solution in their model.

The equation set has several dependencies that preclude a fully implicit solution for θ_i^{n+1}, q_i^{n+1}, $T_{\ell sun,i}^{n+1}$, $T_{\ell sha,i}^{n+1}$, and T_0^{n+1}. Net radiation depends on leaf and ground temperatures. Ryder et al. (2016) avoided this by specifying longwave emission as an implicit term in the energy balance equation, but there are other complicating factors. Boundary layer conductance is calculated from wind speed, but also air and leaf temperatures (to account for free convection using the Grashof number). The wet and dry fractions of the canopy vary with evaporative flux. Wind speed and aerodynamic conductances depend on the surface layer stability as quantified by the Obukhov length, yet this length scale depends on the surface fluxes. Stomatal conductance requires leaf temperature, air temperature, and water vapor concentration. Further complexity to the canopy flux calculations arises because stomatal conductance is calculated from principles of water transport along the soil–plant–atmosphere continuum such that leaf water potential cannot drop below some threshold (Williams et al., 1996; Bonan et al., 2014). This requires the leaf transpiration flux, which itself depends on stomatal conductance. The CLM4.5 has similar dependences in its surface flux calculation and solves the fluxes in a numerical procedure with

Deleted: source

297 up to 40 iterations for a single model timestep. Instead, we solve the equations using a 5-minute
298 sub-timestep to evaluate fluxes over a full model timestep (30 minutes when coupled to an
299 atmospheric model). In the sub-timestep looping, the current values of wind speed, temperature,
300 water vapor concentration, and canopy water are used to calculate the leaf and aerodynamic
301 conductances needed to update the flux–profiles.
302
303 **2.2 Plant canopy and roughness sublayer**
304 The solution to the scalar fluxes and profiles described in the preceding section requires the
305 aerodynamic conductance (g_a), and also wind speed (u) to calculate leaf boundary layer
306 conductance (g_b). These are provided by the RSL parameterization. We follow the theory of
307 Harman and Finnigan (2007, 2008). In their notation, the coordinate system is defined such that
308 the vertical origin is the top of the canopy and z is the deviation from the canopy top. Here, we
309 retain z as the physical height above the ground, whereby $z-h$ is the deviation from the
310 canopy top. The Harman and Finnigan (2007, 2008) parameterization modifies the MOST
311 profiles of u , θ , and q above plant canopies for the RSL and does not require a multi-layer
312 canopy (e.g., Harman, 2012), but was derived by coupling the above-canopy momentum and
313 scalar fluxes with equations for the momentum and scalar balances within a dense, horizontally
314 homogenous canopy. Here, we additionally utilize the within-canopy equations.
315 Neglecting the RSL, the wind speed profile is described by MOST as
316 $$u(z)=\frac{u_*}{k}\left[\ln\left(\frac{z-d}{z_0}\right)-\psi_m\left(\frac{z-d}{L_{MO}}\right)+\psi_m\left(\frac{z_0}{L_{MO}}\right)\right] \quad (18)$$
317 where u_* is friction velocity (m s^{-1}), z is height above the ground (m), d is displacement height
318 (m), z_0 is roughness length (m), and the similarity function ψ_m adjusts the log profile in relation

to the Obukhov length (L_{MO} , m). The Harman and Finnigan (2007, 2008) RSL parameterization reformulates this as

$$u(z)=\frac{u_*}{k}\left[\ln\left(\frac{z-d}{h-d}\right)-\psi_m\left(\frac{z-d}{L_{MO}}\right)+\psi_m\left(\frac{h-d}{L_{MO}}\right)+\hat{\psi}_m\left(\frac{z-d}{L_{MO}},\frac{z-d}{l_m/\beta}\right)-\hat{\psi}_m\left(\frac{h-d}{L_{MO}},\frac{h-d}{l_m/\beta}\right)+\frac{k}{\beta}\right] \quad (19)$$

This equation is analogous to the previous equation, but is valid only for wind speed above the canopy at heights $z \geq h$. It rewrites Eq. (18) so that the lower surface is the canopy height (h , m) rather than the apparent sink for momentum ($d + z_0$). This eliminates z_0 , but introduces $u(h)$ (the wind speed at the top of the canopy) as a new term, which is specified by $\beta = u_* / u(h)$. Eq. (19) also introduces $\hat{\psi}_m$, which adjusts the profile to account for canopy-induced physics in the RSL. Whereas ψ_m uses the length scale L_{MO} , $\hat{\psi}_m$ introduces a second length scale l_m / β . The length scale l_m / β is the dominant scale of the shear-driven turbulence generated at or near the canopy top, is equal to $u / (\partial u / \partial z)$ at the top of the canopy, and relates to canopy density. The corresponding equation for temperature above the canopy is

$$\theta(z)-\theta(h)=\frac{\theta_*}{k}\left[\ln\left(\frac{z-d}{h-d}\right)-\psi_c\left(\frac{z-d}{L_{MO}}\right)+\psi_c\left(\frac{h-d}{L_{MO}}\right)+\hat{\psi}_c\left(\frac{z-d}{L_{MO}},\frac{z-d}{l_m/\beta}\right)-\hat{\psi}_c\left(\frac{h-d}{L_{MO}},\frac{h-d}{l_m/\beta}\right)\right] \quad (20)$$

with θ_* a temperature scale (K) and ψ_c and $\hat{\psi}_c$ corresponding functions for scalars. The same equation applies to water vapor, but substituting q and q_* . The new terms in the profile equations introduced by the RSL theory are: β , the ratio of friction velocity to wind speed at the canopy height; l_m , the mixing length (m) in the canopy; and the modified similarity functions $\hat{\psi}_m$ and $\hat{\psi}_c$. Expressions for these are obtained by considering the momentum and scalar balances within a dense, horizontally homogenous canopy and by matching the above- and within-canopy profile equations at the canopy height h (Appendix A2). In addition, the RSL

Deleted: is

theory provides an equation for d, rather than specifying this as an input parameter. Eq. (20) also requires $\theta(h)$, the air temperature (K) at the canopy height. Harman and Finnigan (2008) provide an equation that relates this to the bulk surface temperature (θ_s) for use with a bulk surface parameterization. Here, we treat $\theta(h)$ as a prognostic variable obtained for the top canopy layer as described in the previous section.

With the assumption of a constant mixing length (l_m) in the canopy, wind speed within the canopy at heights $z \le h$ follows an exponential decline with greater depth in the canopy in relation to the height $z-h$ normalized by the length scale l_m / β, with

$$u(z) = u(h)\exp\left[\frac{z-h}{l_m/\beta}\right] \tag{21}$$

This is the same equation derived by Inoue (1963) and Cionco (1965), but they express the exponential term as $-\eta(1-z/h)$, where η is an empirical parameter. Harman and Finnigan (2007, 2008) introduced the notation l_m / β, whereby $\eta / h = \beta / l_m$, so that the exponential decay of wind speed in the canopy relates to the RSL. The wind speed profile matches Eq. (19) at the top of the canopy through $u(h)$. We restrict $u \ge 0.1$ m s^{-1} (see Discussion for further details). The corresponding profile for the scalar diffusivity within the canopy is similar to that for wind with

$$K_c(z) = K_c(h)\exp\left[\frac{z-h}{l_m/\beta}\right] \tag{22}$$

In the RSL theory of Harman and Finnigan (2008),

$$K_c(h) = l_m u_* / S_c \tag{23}$$

where the Schmidt number (S_c) is defined as the ratio of the diffusivities for momentum and scalars at the top of the canopy (Appendix A2). The diffusivity of water vapor is assumed to

equal that for heat as in Harman and Finnigan (2008). Eq. (21) for u and Eq. (22) for K_c are derived from first-order turbulence closure with constant mixing length in the canopy. They have been used previously to parameterize within-canopy wind and scalar diffusivity in plant canopy models (Shuttleworth and Wallace, 1985; Choudhury and Monteith, 1988), land surface models (Dolman, 1993; Bonan, 1996; Niu and Yang, 2004), and hydrologic models (Mahat et al., 2013; Clark et al., 2015), but without the RSL and with η specified as a model parameter.

The aerodynamic conductance for scalars at level i above the canopy ($z > h$) between heights z_i and z_{i+1} is

$$g_{a,i} = \rho_m k u_* \left[\ln\left(\frac{z_{i+1}-d}{z_i-d}\right) - \psi_c\left(\frac{z_{i+1}-d}{L_{MO}}\right) + \psi_c\left(\frac{z_i-d}{L_{MO}}\right) + \hat{\psi}_c\left(z_{i+1}\right) - \hat{\psi}_c\left(z_i\right) \right]^{-1} \tag{24}$$

where $\hat{\psi}_c$ is evaluated at z_i and z_{i+1}. The conductance within the canopy ($z < h$) consistent with the RSL theory is obtained from Eq. (22) as

$$\frac{1}{g_{a,i}} = \frac{1}{\rho_m} \int_{z_i}^{z_{i+1}} \frac{dz}{K_c(z)} \tag{25}$$

so that

$$\frac{1}{g_{a,i}} = \frac{1}{\rho_m} \frac{S_c}{\beta u_*} \left\{ \exp\left[-\frac{(z_i - h)}{l_m / \beta} \right] - \exp\left[-\frac{(z_{i+1} - h)}{l_m / \beta} \right] \right\} \tag{26}$$

For the top canopy layer, the conductance is integrated between the heights z_i and h, and the above-canopy conductance from h to z_{i+1} is additionally included. The conductance immediately above the ground is

$$g_{a,0} = \rho_m k^2 u_1 \left[\ln\left(\frac{z_1}{z_{0m,g}}\right) \ln\left(\frac{z_1}{z_{0c,g}}\right) \right]^{-1} \tag{27}$$

with $z_{0m,g} = 0.01$ m and $z_{0c,g} = 0.1 z_{0m,g}$ the roughness lengths of the ground for momentum and scalars, respectively, as in the CLM4.5 and assuming neutral stability in this layer. In calculating the conductances, we use the constraint $\rho_m / g_{a,i} \leq 500$ s m^{-1} (see Discussion for further details).

Harman and Finnigan (2007, 2008) provide a complete description of the RSL equations and their derivation. Appendix A2 gives the necessary equations as implemented herein. Use of the RSL parameterization requires specification of the Monin–Obukhov functions ψ_m and ψ_c, the RSL functions $\hat{\psi}_m$ and $\hat{\psi}_c$, and equations for β and S_c. Expressions for l_m and d are obtained from β. Solution to the RSL parameterization requires an iterative calculation for the Obukhov length (L_{MO}) as shown in Figure 2 and explained further in Appendix A3. The equations as described above apply to dense canopies. Appendix A4 gives a modification for sparse canopies.

2.3 Plant area density

Land surface models commonly combine leaf and stem area into a single plant area index to calculate radiative transfer, and the CLM4.5 does the same. By using plant area index, big-leaf canopy models assume that woody phytoelements (branches, stems) are randomly interspersed among leaves. Some studies of forest canopies suggest that branches and stems are shaded by foliage and therefore contribute much less to obscuring the sky than if they were randomly dispersed among foliage (Norman and Jarvis, 1974; Kucharik et al., 1998). To allow for shading, we represent plant area density as separate profiles of leaf and stem area. The beta distribution probability density function provides a continuous profile of leaf area density for use with multi-layer canopy models, and we use a uniform profile for stem area, whereby

$$a(z) = \frac{L_T}{h} \frac{(z/h)^{p-1}(1-z/h)^{q-1}}{\mathrm{B}(p,q)} + \frac{S_T}{h} \quad (28)$$

The first term on the right-hand side is the leaf area density with z/h the relative height in the canopy and L_T leaf area index (m^2 m^{-2}). The beta function (B) is a normalization constant. The parameters p and q determine the shape of the profile (Figure 3). Representative values are $p = q = 2.5$ for grassland and cropland, $p = 3.5$ and $q = 2.0$ for deciduous trees and spruce trees, and $p = 11.5$ and $q = 3.5$ for pine trees (Meyers et al., 1998; Wu et al., 2003). The second term on the right-hand side is the stem area density calculated from the stem area index of the canopy (S_T). For these simulations, L_T comes from tower data , and S_T is estimated from L_T as in the CLM4.5.

2.4 Leaf heat capacity

The CLM4.5 requires specific leaf area as an input parameter, and we use this to calculate leaf heat capacity (per unit leaf area). Specific leaf area, as used in the CLM4.5, is the area of a leaf per unit mass of carbon (m^2 g^{-1} C) and is the inverse of leaf carbon mass per unit area (M_a, g C m^{-2}). This latter parameter is converted to dry mass assuming the carbon content of dry biomass is 50% so that the leaf dry mass per unit area is M_a / f_c with f_c = 0.5 g C g^{-1}. The leaf heat capacity (c_L, J m^{-2} K^{-1}) is calculated from leaf dry mass per unit area after adjusting for the mass of water, as in Ball et al. (1988) and Blanken et al. (1997). Following Ball et al. (1988), we assume that the specific heat of dry biomass is one-third that of water (c_{dry} = 1.396 J g^{-1} K^{-1}). Then, with f_w the fraction of fresh biomass that is water, the leaf heat capacity is

$$c_L = \frac{M_a}{f_c} c_{dry} + \frac{M_a}{f_c}\left(\frac{f_w}{1-f_w}\right) c_{wat} \quad (29)$$

The first term on the right-hand side is the mass of dry biomass multiplied by the specific heat of dry biomass. The second term is the mass of water multiplied by the specific heat of water (c_{wat} = 4.188 J g^{-1} K^{-1}). We assume that 70% of fresh biomass is water (f_w = 0.7 g H_2O g^{-1}). Niinemets (1999) reported a value of 0.66 g H_2O g^{-1} in an analysis of leaves from woody plants. The calculated heat capacity for grasses, crops, and trees is 745–2792 J m^{-2} K^{-1} depending on specific leaf area (Table 1). For comparison, Blanken et al. (1997) calculated a heat capacity of 1999 J m^{-2} K^{-1} for aspen leaves with a leaf mass per area of 111 g m^{-2} and f_w = 0.8. Ball et al. (1988) reported a range of 1100–2200 J m^{-2} $K^{-1}$for mangrove leaves spanning a leaf mass per area of 93–189 g m^{-2} with f_w = 0.71.

3 Model evaluation

Deleted: simulations

3.1 Flux tower data

We evaluated the canopy model at 12 AmeriFlux sites comprising 81 site-years of data using the same protocol of the earlier model development (Bonan et al., 2014). We used the 6 forests sites previously described in Bonan et al. (2014) and included additional flux data for 1 forest (US-Dk2), 2 grassland (US-Dk1, US-Var), and 3 cropland sites (US-ARM, US-Bo1, US-Ne3) to test the canopy model over a range of tall and short canopies, dense and sparse leaf area index, and different climates (Table 2). Tower forcing data (downwelling solar and longwave radiation, air temperature, relative humidity, wind speed, surface pressure, precipitation, and tower height) were from the North American Carbon Program (NACP) site synthesis (Schaefer et al., 2012) as described previously (Bonan et al., 2014), except as noted below for the three Duke tower sites.

The model was evaluated using tower observations of net radiation, sensible heat flux, latent heat flux, and friction velocity obtained from the AmeriFlux Level 2 data set (ameriflux.lbl.gov) and with gross primary production from the NACP site synthesis (Schaefer et al., 2012). The tower forcing and fluxes have a resolution of 30 minutes except for four sites (US-Ha1, US-MMS, US-UMB, US-Ne3) with 60-minute resolution. We limited the simulations to one particular month (with the greatest leaf area) in which soil moisture was prescribed as in Bonan et al. (2014) so as to evaluate the canopy physics parameterizations without confounding effects of seasonal changes in soil water.

Ryu et al. (2008) describe the US-Var grassland located in California. The CLM has been previously tested using flux data from the US-Ne3 and US-Bo1 cropland sites (Levis et al., 2012), and we used the same sites here. The US-Ne3 tower site is a rainfed maize (*Zea mays*) – soybean (*Glycine max*) rotation located in Nebraska (Verma et al., 2005). We used flux data for soybean, a C_3 crop (years 2002 and 2004). Kucharik and Twine (2007) give leaf area index, also in the AmeriFlux biological, ancillary, disturbance and metadata. The same ancillary data show a canopy height of 0.9 m during August for soybean. The US-Bo1 site is a maize–soybean rotation located in Illinois (Meyers and Hollinger, 2004; Hollinger et al., 2005). Meyers and Hollinger (2004) give canopy data. We used a leaf area index of 5 m^2 m^{-2} and canopy height of 0.9 m for soybean (1998–2006, even years). Flux data for the US-ARM winter wheat site, used to test the CLM4.5, provides an additional dataset with which to test the model (Lu et al., 2017).

Stoy et al. (2006) provide site information for the US-Dk2 deciduous broadleaf forest tower site located in the Duke Forest, North Carolina, which was included here to contrast the adjacent evergreen needleleaf forest and grassland sites. The US-Dk1 tower site in the Duke Forest

provides an additional test for grassland (Novick et al., 2004; Stoy et al., 2006). Tower forcing and flux data for 2004–2008 were as in Burakowski et al. (2018).

3.2 Model simulations

We performed several model simulations to compare the CLM4.5 with the RSL enabled multi-layer canopy. The CLM4.5 and the multi-layer canopy differ in several ways (Table 3). To facilitate comparison and to isolate specific model differences, we devised a series of simulations to incrementally test parameterizations changes (Table 4). The simulations discussed herein are:

1. CLM4.5 – Simulations with the CLM4.5 using tower meteorology and site data for leaf area index, stem area index, and canopy height.
2. m0 – This uses the multi-layer canopy, but configured to be similar to the CLM4.5 for leaf biophysics as described in Table 3. Stomatal conductance is calculated as in the CLM4.5. Leaf nitrogen declines exponentially with greater cumulative plant area index from the canopy top with the decay coefficient $K_n = 0.3$ as in the CLM4.5. The nitrogen profile determines the photosynthetic capacity at each layer so that leaves in the upper canopy have greater maximum photosynthetic rates than leaves in the lower canopy. In addition, leaf and stem area are comingled in the CLM4.5, and there is no heat storage in plant biomass. These features are replicated by having a uniform plant area density profile and by setting leaf heat capacity to a small, non-zero number. This simulation excludes a turbulence parameterization so that air temperature, water vapor concentration, and wind speed in the canopy are equal to the reference height forcing. Juang et al. (2008) referred to this as the well-mixed assumption. In this configuration, the fluxes of sensible and latent heat above the canopy are

Deleted: and to incrementally evaluate the effect of specific processes on model performance

Deleted: summarizes the major model differences, and

Deleted: summarizes the model simulations

the sum of the source/sink fluxes in the canopy, and friction velocity is not calculated. This is the baseline model configuration.

3. m1 – As in m0, but introducing a turbulence closure in the absence of the RSL. Eqs. (16) and (17) are used to calculate θ and q. The CLM4.5 MOST parameterization is used to calculate u and g_a above the canopy. Within the canopy, the mixing length model with exponential profiles for u and g_a as in Eqs. (21) and (26) is used, but with $\eta = 3$, which is a representative value found in many observational studies of wind speed in plant canopies (Thom, 1975; Cionco, 1978; Brutsaert, 1982).

The multi-layer canopy model has several changes to leaf biophysics compared with the CLM4.5. These differences are individually examined in the simulations:

4. b1 – As in m1, but with stomatal conductance calculated using water-use efficiency and plant hydraulics as in Bonan et al. (2014).
5. b2 – As in b1, but with K_n dependent on photosynthetic capacity ($V_{c\max}$) as in Bonan et al. (2014).
6. b3 – As in b2, but with plant area density calculated from Eq. (28).
7. b4 – As in b3, but with leaf heat capacity from Eq. (29). This represents the full suite of parameterization changes prior to inclusion of the RSL. We refer to this simulation also as ML-RSL.

The final two simulations examine the RSL:

8. r1 – As in b4, but with the RSL parameterization used to calculate u and g_a above the canopy using Eqs. (19) and (24). In this configuration, the CLM4.5 MOST parameterization is replaced by the RSL parameterization for above-canopy profiles, but $\eta = 3$ for within canopy profiles.

9. r2 – As in r1, but u and g_a in the canopy are calculated from the RSL parameterization using l_m / β rather than $\eta = 3$. This is the full ML+RSL configuration, and comparison with ML-RSL shows the effects of including the RSL parameterization.

Simulations were evaluated in terms of net radiation, sensible heat flux, latent heat flux, gross primary production, friction velocity, and radiative temperature. Radiative temperature for both the observations and simulations was evaluated from the upward longwave flux using an emissivity of one. The simulations were assessed in terms of root mean square error (RMSE) for each of the 81 site–years. We additionally assessed model performance using Taylor diagrams and the corresponding skill score (Taylor, 2001) as in Bonan et al. (2014). Taylor diagrams quantify the degree of similarity between the observed and simulated time series of a particular variable in terms of the correlation coefficient (r) and the standard deviation of the model data relative to that of the observations ($\hat{\sigma}$). The Taylor skill score combines these two measures into a single metric of model performance with a value of one when $r = 1$ and $\hat{\sigma} = 1$.

4 Results

4.1 Model evaluation

The ML+RSL simulation has better skill compared with CLM4.5 at most sites and for most variables (Table 5). Of the 7 forest sites, net radiation (R_n) is improved at 5 sites, sensible heat flux (H) at 5 sites, latent heat flux (λE) at 4 sites, friction velocity (u_*) at 6 sites, radiative temperature (T_{rad}) at the 5 sites with data, and gross primary production (GPP) at 3 of the 5 sites with data. H is improved at all 5 herbaceous sites, λE at 3 sites, u_* at 3 sites, T_{rad} at 4 sites, and GPP at the 2 sites with data. R_n generally is unchanged at the herbaceous sites.

Simulations for US-UMB illustrate these improvements for the forest sites, where the influence of the RSL is greatest. For July 2006, CLM4.5 overestimates mid-day H and underestimates mid-day GPP (Figure 4). Mid-day latent heat flux is biased low, but within the measurement error. u_* is underestimated at night, and T_{rad} has a larger diurnal range with colder temperatures at night and warmer temperatures during the day compared with the observations. ML+RSL improves the simulation. Mid-day H decreases and GPP increases, nighttime u_* increases, and the diurnal range of T_{rad} decreases. Taylor diagrams for all years (1999–2006; Figure 5) show improved H, λE, and GPP (in terms of the variance of the modeled fluxes relative to the observations), u_* (in terms of correlation with the observations), and T_{rad} (both variance and correlation). Similar improvements are seen at the other forest sites.

Figure 6 shows the relationship between H and the temperature difference between the surface and reference height ($T_{rad} - T_{ref}$) for two forest sites (US-UMB and US-Me2) and one crop site (US-ARM). These sites were chosen because the root mean square error of the model (ML+RSL) is low for H and T_{rad}. The observations show a positive correlation between $T_{rad} - T_{ref}$ and H beginning at about –2 °C. CLM4.5 and ML+RSL capture this relationship, but the slope at the forest sites is smaller for CLM4.5 than for ML+RSL and the CLM4.5 data have more scatter. For stable conditions ($H < 0$), CLM4.5 shows a slight linear increase in sensible heat transfer to the surface (US-UMB) or is nearly invariant (US-Me2) as T_{rad} becomes progressively colder than T_{ref}. ML+RSL better captures the observations, particularly the more negative H as $T_{rad} - T_{ref}$ approaches zero. CLM4.5 also has a wider range of temperatures compared with the observations and ML+RSL at the forest sites. The primary effect of the RSL

Deleted: The observations have a distinct relationship between H and the temperature difference between the surface and reference height ($T_{rad} - T_{ref}$), as shown in

Deleted: where

Deleted: The observations show a complex relationship between temperature and H f

Deleted: . At the forest sites

is to reduce high daytime temperatures and to increase sensible heat transfer to the surface at night. Model differences are less at US-ARM.

Deleted: Both models perform similarly

4.2 Effect of specific parameterizations

Comparisons of ML-RSL and ML+RSL for US-UMB (July 2006) show improvements in the multi-layer canopy even without the RSL parameterization (Figure 4). ML-RSL reduces mid-day H, increases mid-day λE and GPP, and reduces the diurnal range of T_{rad}. The nighttime bias in u_* also decreases. Inclusion of the RSL (ML+RSL) further improves u_* and T_{rad}, but slightly degrades H by increasing the daytime peak.

Comparison of the suite of simulations (m0 to r2; Table 4) for forest sites highlights the effect of specific parameterization changes on model performance. The m0 simulation without a turbulence closure has high RMSE compared with CLM4.5 for λE (Figure 7) and H (Figure 8). Inclusion of a turbulence closure (above-canopy, CLM4.5 MOST; within-canopy, mixing length model) in m1 substantially reduces RMSE compared with m0 at all sites. The m1 RMSE for λE is reduced compared with CLM4.5 at 5 of the 7 sites and for H at 4 sites. The leaf biophysical simulations (b1–b4) reduce λE RMSE compared with m1 at 6 sites (US-Ho1 is the exception), and the RMSE also decreases compared with CLM4.5 (Figure 7). Among b1–b4, the biggest effect on λE RMSE occurs from stomatal conductance and nitrogen profiles (b1 and b2). The RSL parameterization (r1 and r2) has relatively little additional effect on RMSE. The leaf biophysical simulations (b1–b4) have a similar effect to reduce RMSE for H compared with m1, and RMSE decreases compared with CLM4.5 (Figure 8). Inclusion of the RSL (r1 and r2) degrades H in terms of RMSE. Whereas the b4 simulation without the RSL parameterization decreases RMSE compared with CLM4.5, this reduction in RMSE is lessened in r1 and r2. The

589 RMSE for u_* in m1 decreases compared with CLM4.5 at all sites (Figure 9). The leaf biophysics
590 simulations have little effect on RMSE, but the RSL simulations (r1 and r2) further reduce
591 RMSE. The m0 simulation without a turbulence closure has substantially lower RMSE for T_{rad}
592 compared with the other simulations (Figure 10). This is seen in an improved simulation of the
593 diurnal temperature range, with warmer nighttime minimum and cooler daytime maximum
594 temperatures compared with the other simulations (not shown). The m1 simulation increases
595 RMSE, but RMSE is still reduced compared with CLM4.5 at the 5 sites with data. The leaf
596 biophysical simulations (b1–b4) have little effect on T_{rad} , but the RSL simulations reduce
597 RMSE, more so for r1 than r2.
598
599 **4.3 Canopy profiles**
600 Leaf temperature profiles are consistent with the changes in T_{rad} , as shown in Figure 11 for US-
601 UMB. The m0 simulation has the coolest daytime and warmest nighttime leaf temperatures.
602 Inclusion of a turbulence closure (m1) warms daytime temperatures and cools nighttime
603 temperatures. The leaf biophysics (b4) reduces the m1 temperature changes, and the RSL
604 simulations (r1 and r2) further reduce the changes.
605 Wind speed and temperature profiles simulated with the RSL parameterization are
606 noticeably different compared with MOST profiles, as shown in Figure 12 for US-UMB. At mid-
607 day, wind speed in the upper canopy is markedly lower than for MOST, but whereas wind speed
608 goes to zero with MOST, the RSL wind speed remains finite. Mid-day MOST air temperature in
609 the canopy increases monotonically to a maximum of 28.5 °C, but the RSL produces a more
610 complex profile with a temperature maximum of about 26.5 °C in the mid-canopy and lower
611 temperatures near the ground. During the night, the upper canopy cools to a temperature of about

Deleted: these results

613 15 °C, but temperatures in the lower canopy remain warm. The other forest sites show similar
614 profiles.
615
616 **5 Discussion**
617 The multi-layer canopy with the RSL (ML+RSL) improves the simulation of surface fluxes
618 compared to the CLM4.5 at most forest and herbaceous sites (Table 5). In terms of λE, the
619 turbulence closure using the CLM4.5 MOST above the canopy and a mixing length model in the
620 canopy (with $\eta = 3$) substantially reduces RMSE compared to the well-mixed assumption in
621 which the canopy has the same temperature, water vapor concentration, and wind speed as the
622 reference height (m0, m1; Figure 7). A similar result is seen for H (Figure 8). This finding is
623 consistent with Juang et al. (2008), who showed that first-order turbulence closure improves
624 simulations in a multi-layer canopy compared with the well-mixed assumption.
625 Additional improvement in λE comes from the leaf biophysics (particularly stomatal
626 conductance and photosynthetic capacity) (b1, b2; Figure 7). This is consistent with Bonan et al.
627 (2014), who previously showed improvements arising from the multi-layer canopy, stomatal
628 conductance, and photosynthetic capacity at the forest sites. Differences between the CLM4.5
629 and ML+RSL stomatal models likely reflects differences in parameters (slope g_1 for CLM4.5;
630 marginal water-use efficiency ι for ML+RSL) rather than model structure (Franks et al., 2017).
631 Further differences arise from the plant hydraulics (Bonan et al., 2014). The RSL has
632 comparatively little effect on λE (r1, r2; Figure 7). H is similarly improved by the leaf
633 biophysics, but is degraded by the RSL (Figure 8) because of an increase in the peak mid-day
634 flux. Harman (2012) also found that the RSL has negligible effect on λE because this flux is
635 dominated by stomatal conductance, but increases the peak H.

636 The influence of the RSL is evident in the improved relationship between H and the
637 surface–air temperature difference ($T_{rad} - T_{ref}$) at forest sites (Figure 6). In the CLM4.5, a larger
638 temperature difference is needed to produce the same positive heat flux to the atmosphere
639 compared with the observations. With the RSL, a smaller temperature difference gives the same
640 sensible heat flux, comparable to the observations. This is expected from the RSL theory because
641 of the larger aerodynamic conductance. Additional improvement, as expected from the RSL
642 theory, is seen during moderately stable periods, which in turn reduces surface cooling. Similar
643 such improvement is not seen at the shorter crop site (US-ARM).

Deleted: because the measurements were taken above the RSL

644 The influence of the RSL is also evident in nighttime u_* (Figure 4). Substantial reduction
645 in RMSE is seen in the m1 simulation (Figure 9), which closely mimics the CLM4.5 in terms of
646 leaf biophysics and use of MOST above the canopy. The different numerical methods used
647 between the multi-layer canopy and the CLM4.5 to solve for canopy temperature, surface fluxes,
648 and the Obukhov length may explain the poor CLM4.5 simulations. The RSL parameterization
649 further improves u_* (r1, r2; Figure 9), primarily by increasing u_* at night as expected due to
650 shear-driven turbulence induced by the canopy dominating during night compared with day.

651 Another outcome of the RSL in seen in T_{rad} and leaf temperature. The lowest RMSE
652 occurs with the well-mixed approximation (m0; Figure 10), which also produces the coolest
653 daytime and warmest nighttime leaf temperatures (m0; Figure 11). Adding a turbulence closure
654 (m1) substantially warms daytime leaf temperatures and cools nighttime temperatures, which
655 degrades the T_{rad} RMSE. The RSL (r1, r2) decreases the daytime temperatures and warms the
656 nighttime temperatures, which improve the RMSE. Leaf temperatures are cooler during the day
657 and warmer at night compared with the CLM4.5. Overall, the diurnal temperature range
658 improves in the ML+RSL simulation compared to that from the CLM4.5, seen in both the

660 nighttime minimum and the daytime maximum of T_{rad} (Figure 4). This latter improvement is
661 particularly important given the use of radiometric land surface temperature as an indicator of the
662 climate impacts of land cover change (Alkama and Cescatti, 2016).

663 The simulation of wind and temperature profiles is a key outcome of the multi-layer
664 canopy and RSL. During the day, the CLM4.5 simulates a warmer canopy air space than the
665 ML+RSL simulation (Figure 12). Air temperature obtained from MOST increases monotonically
666 towards the bulk surface, whereas the ML+RSL simulation produces a more complex vertical
667 profile with a maximum located in the upper canopy and cooler temperatures in the lower
668 canopy. Geiger (1927) first described such profiles, seen also in some studies (Jarvis and
669 McNaughton, 1986; Pyles et al., 2000; Staudt et al., 2011). The simulated nighttime temperatures
670 are warmer than the CLM4.5. Temperature profiles have a minimum in the upper canopy, above
671 which temperature increases with height. However, temperatures increase in the lower canopy.
672 Nighttime temperatures in a walnut orchard show a minimum in the upper canopy arising from
673 radiative cooling, but the temperature profile in the lower canopy is more uniform than seen in
674 Figure 12 (Patton et al., 2011). Enhanced diffusivity resulting from convective instability in the
675 canopy makes the temperature profile more uniform in the Patton et al. (2011) observations; this
676 process is lacking in the RSL parameterization. Ryder et al. (2016) and Chen et al. (2016) noted
677 the difficulty in modeling nighttime temperature profiles in forests and introduced in
678 ORCHIDEE-CAN an empirical scaling factor to K_c that varies between day and night. The
679 results of the present study, too, suggest that turbulent mixing in conditions where the
680 stratification within and above the canopy differ in sign needs additional consideration. The
681 importance of within-canopy temperature gradients is seen in forest canopies. The microclimatic
682 influence of dense forest canopies buffers the impact of macroclimatic warming on understory

Deleted: over the day

Deleted: that t

685 plants (De Frenne et al., 2013), and the vertical climatic gradients in tropical rainforests are
686 steeper than elevation or latitudinal gradients (Scheffers et al., 2013).

687 Various ad hoc changes have been introduced into the next version of the Community
688 Land Model (CLM5) to correct the deficiencies in u_* and T_{rad}. In particular, the Monin–
689 Obukhov stability parameter has been constrained in stable conditions so that $(z-d)/L_{MO} \le 0.5$.
690 This change increases nighttime u_*, increases sensible heat transfer to the surface at night, and
691 increases nighttime T_{rad} (not shown). In contrast, the ML+RSL simulation reduces these same
692 biases, but resulting from a clear theoretical basis describing canopy-induced physics.

693 The canopy model encapsulates conservation equations for θ and q, the energy balance
694 for the sunlit and shaded canopy, and the ground surface energy balance. The various terms in
695 Eqs. (16) and (17), the governing equations, are easily derived from flux equations and relate to
696 the leaf (g_b, $g_{\ell sun}$, $g_{\ell sha}$) and aerodynamic (g_a) conductances, leaf and canopy air storage terms
697 (c_L, $\rho_m \Delta z / \Delta t$), plant area index and the sunlit fraction (ΔL, f_{sun}), net radiation ($R_{n\ell sun}$, $R_{n\ell sha}$),
698 and soil surface (R_{n0}, h_{s0}, g_{s0}, κ_{soil}, T_{soil}). These are all terms that need to be defined in land
699 surface models (except for the storage terms which are commonly neglected), and so the only
700 new term introduced into the flux equations is leaf heat capacity, but that is obtained from the
701 leaf mass per area, which is a required parameter in the CLM4.5.

702 The Harman and Finnigan (2007, 2008) RSL parameterization provides the necessary
703 aerodynamic conductances and wind speed. It produces a comparable representation of surface-
704 atmosphere exchange of heat, water and carbon, including within-canopy exchange, to those
705 based on Lagrangian dynamics (e.g., McNaughton and van den Hurk, 1995) and localized near-
706 field theory (e.g., Raupach, 1989; Raupach et al., 1997; Siqueira et al., 2003; Ryder et al., 2016;

Chen et al., 2016). Lagrangian representations have the advantage in that they retain closer fidelity to the underlying dynamics governing exchange. In contrast, however, the RSL formulation provides linked representations for both momentum and (passive) scalar exchange. This coupling, impossible with Lagrangian formulations as there is no locally-conserved equivalent quantity to scalar concentration for momentum, reduces the degrees of freedom involved. The RSL's linked formulation also facilitates the propagation of knowledge about the transport of one quantity onto the transport of all other quantities considered. Unlike Lagrangian formulations, the RSL formulation also naturally asymptotes towards the standard surface layer representations as required, e.g., with increasing height above ground or for short canopies.

Furthermore, the components of the RSL formulation are far easier to observe than those in the Lagrangian representations. In particular, the vertical profile of the Lagrangian time scale (T_L), critical to the localized near-field formulation, is extremely difficult to determine from observations or higher-order numerical simulations. Most understanding around T_L is indirect, heuristic, or tied to an inverted model (Massman and Weil, 1999; Haverd et al., 2009). Finally, it is worth noting that the RSL formulation is derived from the scales of the coherent and dominant turbulent structures and directly incorporates canopy architecture (Raupach et al., 1996; Finnigan et al., 2009), thereby permitting future adaptation of the formulation to advances in our understanding of the structure and role of turbulence, e.g. to variation with canopy architecture, landscape heterogeneity, or in low wind conditions. Far greater effort would be required to update the parameterizations of the components in the Lagrangian representations to advances in the understanding of turbulence.

The Harman and Finnigan (2007, 2008) RSL parameterization eliminates a priori specification of roughness length and displacement height, but introduces other parameters.

730 Critical parameters are the drag coefficient of canopy elements in each layer ($c_d = 0.25$), the
731 value of $u_* / u(h)$ for neutral conditions ($\beta_N = 0.35$), and the Schmidt number at the canopy top
732 with a nominal value $S_c = 0.5$ as modified for atmospheric stability using Eq. (54). These
733 parameters have physical meaning, are largely observable, have a well-defined range of observed
734 values, and are not unconstrained parameters to fit the model to observations. The expressions
735 for β and S_c given by Eqs. (51) and (54) are observationally-based, but nevertheless are
736 heuristic (Harman and Finnigan, 2007, 2008). The parameter c_2 relates to the depth scale of the
737 RSL and though c_2 can have complex expressions, a simplification is to take $c_2 = 0.5$ (Harman
738 and Finnigan, 2007, 2008; Harman, 2012). The canopy length scale L_c is assumed to be constant
739 with height as in Eq. (56) and is thought to be more conservative than either leaf area density or
740 the leaf drag coefficient separately (Harman and Finnigan (2007). Massman (1997) developed a
741 first-order closure canopy turbulence parameterization that accounts for vertical variation in leaf
742 area density, but that is not considered here.

743 The plant canopies simulated in this study are dense canopies in the sense that most of the
744 momentum is absorbed by plant elements. Appendix A4 provides a modification for sparse
745 canopies (e.g., plant area index < 1 m^2 m^{-2}) whereby β decreases, but this extension to sparse
746 canopies is largely untested. Raupach (1994) and Massman (1997) also decrease β with sparse
747 canopies. We note that the same challenge occurs in land surface models such as the CLM4.5,
748 with parameterizations to account for the effects of canopy denseness on within-canopy
749 turbulence (Zeng et al., 2005).

750 The RSL parameterization has limits to its applicability; L_c / L must be greater than some
751 critical value related to β in unstable conditions and less than some critical value in stable

752 conditions (Harman and Finnigan, 2007). We constrained β to a value between 0.5 (unstable)
753 and 0.2 (stable). In practice, this means that $L_c / L \geq -0.79$ (unstable) and $L_c / L \leq 3.75$ (stable),
754 which satisfies the theoretical limits given by Harman and Finnigan (2007). This range of values
755 for β is consistent with observations above forest canopies shown in Harman and Finnigan
756 (2007) and is comparable with other parameterizations. Data presented by Raupach (1994) show
757 a similar range in β for full plant canopies, and his parameterization has a maximum value of
758 0.3. Massman's (1997) parameterization of β has a maximum value of 0.32 for full canopies,
759 but he notes that other studies suggest a range of 0.15–0.25 to 0.40. The Harman and Finnigan
760 (2007) parameterization used here has the advantage of being consistent with current RSL theory
761 (Raupach et al., 1996; Finnigan et al., 2009) and incorporates stability dependence through β, in
762 contrast with Raupach (1994) and Massman (1997). Removing the lower limit $\beta \geq 0.2$ has little
763 effect on the simulations, while the upper limit $\beta \leq 0.5$ acts to suppress daytime u_* at some sites
764 (not shown).

765 l_m / β is a critical length scale in the RSL theory. It modifies flux–profile relationships
766 ($\hat{\phi}_m$, $\hat{\phi}_c$) and also the profiles for u and K_c in the canopy given by Eqs. (21) and (22). These
767 latter profiles decline exponentially with greater depth in the canopy in relation to l_m / β, which
768 can be equivalently written as $0.5 c_d a / \beta^2$ substituting l_m from Eq. (55) and L_c from Eq. (56).
769 For a particular canopy defined by c_d and $a = (L_T + S_T) / h$, the exponential within-canopy
770 profile is bounded by the limits placed on β. Further insight is gained from an equivalent form
771 of the wind profile equation in which $u(z) = u(h) \exp[-\eta(1 - z/h)]$ with $\eta = h\beta / l_m$. A typical
772 value of η reported in observational studies is 2–4 (Thom, 1975; Cionco, 1978; Brutsaert, 1982).

Comparing equations shows that $\eta = 0.5 c_d (L_T + S_T) / \beta^2$. The constraint $0.2 \le \beta \le 0.5$ places limits to η. The maximum plant area index in our simulations is 7.2 m^2 m^{-2} at US-Dk2. With $c_d = 0.25$, η has values from 3.6 to 22.5. This allows for quite low wind speed and conductance within the canopy. Diabatic stability within the canopy can differ from that above the canopy. This would be reflected in the wind speeds used to calculate the leaf conductances and also the conductance network used to calculate within canopy scalar profiles. For these reasons, we employ minimum values to the within-canopy wind speed and aerodynamic conductances.

6 Conclusion

For over 30 years, land surface models have parameterized surface fluxes using a dual-source canopy in which the vegetation is treated as a big-leaf without vertical structure and in which MOST is used to parameterize turbulent fluxes above the canopy. The RSL parameterization of Harman and Finnigan (2007, 2008) provides a means to represent turbulent processes in a multi-layer model extending from the ground through the canopy and the RSL with sound theoretical underpinnings of canopy-induced turbulence and with few additional parameters. The multi-layer canopy improves model performance compared to the CLM4.5 in terms of latent and sensible heat fluxes, friction velocity, and radiative temperature. Improvement in latent and sensible heat fluxes comes primarily from advances in modeling stomatal conductance and canopy physiology beyond what is in the CLM4.5. These advances also improve friction velocity and radiative temperature, with additional improvement from the RSL parameterization. The multi-layer model combines improvements in both leaf biophysics and canopy-induced turbulence and both contribute to the overall model improvement. Indeed, the modeling of

Deleted: implementation of the RSL

Deleted: , and additional i

canopy turbulence and canopy physiology are inextricably linked (Finnigan and Raupach 1987), and the 30+ years of land surface models has likely lead to compensating insufficiency in both.

Multi-layer canopies are becoming practical for land surface models, seen in the ORCHIDEE-CAN model (Ryder et al., 2016; Chen et al., 2016) and in this study. A multi-layer canopy facilitates the treatment of plant hydraulic control of stomatal conductance (Williams et al., 1996; Bonan et al., 2014), provides new ways to test models directly with leaf-level measurements in the canopy, and is similar to the canopy representations used in canopy-chemistry models (Stroud et al., 2005; Forkel et al., 2006; Wolfe and Thornton, 2011; Ashworth et al., 2015). Here, we provide a tractable means to simulate the necessary profiles of wind speed, temperature, and water vapor while also accounting for the RSL. While this is an advancement over the CLM4.5, much work remains to fully develop this class of model and to implement the multi-layer canopy parameterization in the CLM. Significant questions remain about how well multi-layer models capture the profiles of air temperature, water vapor, and leaf temperature in the canopy, how important these profiles are for vegetation source/sink fluxes, and how many canopy layers are needed to adequately represent gradients in the canopy. The testing of ORCHIDEE-CAN (Chen et al., 2016) has begun to address these questions, but high quality measurements in canopies are required to better distinguish among turbulence parameterizations (e.g., Patton et al., 2011). Moreover, multi-layer canopies raise a fundamental question about the interface between the atmosphere and land surface. The coupling of the Community Land Model with the atmosphere depicts the land as a bulk source/sink for heat, moisture, and momentum, and these fluxes are boundary conditions to the atmosphere model. Multi-layer canopy models simulate a volume of air extending from some level in the

819 atmosphere to the ground. A critical question that remains unresolved is where does the
820 parameterization of the atmospheric boundary layer stop and the land surface model begin.
821
822 **Code availability**
823 The multi-layer canopy runs independent of the CLM4.5, but utilizes common code (e.g., soil
824 temperature). The canopy flux code is available at https://github.com/gbonan/CLM-ml_v0.
825
826 **Appendix A: Model description**
827 **A1 Derivation of Eqs. (16) and (17)**
828 Eq. (10) for the energy balance of the sunlit portion of layer i can be algebraically rewritten as

829 $$T_{\ell sun,i}^{n+1} = \alpha_i^{sun}\theta_i^{n+1} + \beta_i^{sun}q_i^{n+1} + \delta_i^{sun} \tag{30}$$

830 with

831 $$\alpha_i^{sun} = \frac{2c_p g_{b,i}}{2c_p g_{b,i} + \lambda s_i^{sun} g_{\ell sun,i} + c_{L,i}/\Delta t} \tag{31}$$

832 $$\beta_i^{sun} = \frac{\lambda g_{\ell sun,i}}{2c_p g_{b,i} + \lambda s_i^{sun} g_{\ell sun,i} + c_{L,i}/\Delta t} \tag{32}$$

833 $$\delta_i^{sun} = \frac{R_{n\ell sun,i} - \lambda\left[q_{sat}\left(T_{\ell sun,i}^n\right) - s_i^{sun}T_{\ell sun,i}^n\right]g_{\ell sun,i} + c_{L,i}T_{\ell sun,i}^n/\Delta t}{2c_p g_{b,i} + \lambda s_i^{sun} g_{\ell sun,i} + c_{L,i}/\Delta t} \tag{33}$$

834 Similar coefficients are found from Eq. (13) for the shaded leaf to give

835 $$T_{\ell sha,i}^{n+1} = \alpha_i^{sha}\theta_i^{n+1} + \beta_i^{sha}q_i^{n+1} + \delta_i^{sha} \tag{34}$$

836 Eq. (14) for the ground surface energy balance is similarly rewritten as

837 $$T_0^{n+1} = \alpha_0\theta_1^{n+1} + \beta_0 q_1^{n+1} + \delta_0 \tag{35}$$

838 with

839 $$\alpha_0 = \frac{c_p g_{a,0}}{c_p g_{a,0} + \lambda h_{s0} s_0 g_{s0} + \kappa_{soil} / \Delta z_{soil}} \quad (36)$$

840 $$\beta_0 = \frac{\lambda g_{s0}}{c_p g_{a,0} + \lambda h_{s0} s_0 g_{s0} + \kappa_{soil} / \Delta z_{soil}} \quad (37)$$

841 $$\delta_0 = \frac{R_{n0} - \lambda h_{s0}\left[q_{sat}\left(T_0^n\right) - s_0 T_0^n\right] g_{s0} + T_{soil}^n \kappa_{soil} / \Delta z_{soil}}{c_p g_{a,0} + \lambda h_{s0} s_0 g_{s0} + \kappa_{soil} / \Delta z_{soil}} \quad (38)$$

842 With these substitutions, Eqs. (8) and (9) are rewritten as Eqs. (16) and (17) with the algebraic
843 coefficients in Sect. S2 of the Supplement.

844

845 **A2 Roughness sublayer parameterization**

846 The flux–gradient relationships used with Monin–Obukhov similarity theory are

847 $$\phi_m(\zeta) = \begin{cases} (1-16\zeta)^{-1/4} & \zeta < 0 \text{ (unstable)} \\ 1+5\zeta & \zeta \geq 0 \text{ (stable)} \end{cases} \quad (39)$$

848 for momentum, and

849 $$\phi_c(\zeta) = \begin{cases} (1-16\zeta)^{-1/2} & \zeta < 0 \text{ (unstable)} \\ 1+5\zeta & \zeta \geq 0 \text{ (stable)} \end{cases} \quad (40)$$

850 for heat and water vapor. These relationships use the dimensionless parameter $\zeta = (z-d)/L_{MO}$.

851 The integrated similarity functions are

852 $$\psi_m(\zeta) = \begin{cases} 2\ln\left(\frac{1+x}{2}\right) + \ln\left(\frac{1+x^2}{2}\right) - 2\tan^{-1}x + \frac{\pi}{2} & \zeta < 0 \text{ (unstable)} \\ -5\zeta & \zeta \geq 0 \text{ (stable)} \end{cases} \quad (41)$$

853 with $x = (1-16\zeta)^{1/4}$, and

$$\psi_c(\zeta) = \begin{cases} 2\ln\left(\dfrac{1+x^2}{2}\right) & \zeta < 0 \text{ (unstable)} \\ -5\zeta & \zeta \geq 0 \text{ (stable)} \end{cases} \tag{42}$$

These equations are valid for moderate values of ζ from about –2 to 1 (Foken 2006), and we adopt a similar restriction.

The RSL parameterization modifies Monin–Obukhov similarity theory by introducing an additional dimensionless parameter $\xi = (z-d)\beta / l_m$, which is the height $z-d$ normalized by the length scale l_m / β. In Harman and Finnigan (2007, 2008), the modified flux–gradient relationship for momentum is

$$\Phi_m(z) = \phi_m\left(\frac{z-d}{L_{MO}}\right)\hat{\phi}_m\left(\frac{z-d}{l_m/\beta}\right) \tag{43}$$

with

$$\hat{\phi}_m(\xi) = 1 - c_1 \exp(-c_2\xi) \tag{44}$$

and

$$c_1 = \left[1 - \frac{k}{2\beta}\phi_m^{-1}\left(\frac{h-d}{L_{MO}}\right)\right]\exp(c_2/2) \tag{45}$$

and a simplification is to take $c_2 = 0.5$. The integrated RSL function $\hat{\psi}_m$ is

$$\hat{\psi}_m(z) = \int_{z-d}^{\infty} \phi_m\left(\frac{z'}{L_{MO}}\right)\left[1 - \hat{\phi}_m\left(\frac{z'}{l_m/\beta}\right)\right]\frac{dz'}{z'} \tag{46}$$

For scalars, the flux–gradient relationship in Harman and Finnigan (2008) is

$$\Phi_c(z) = \phi_c\left(\frac{z-d}{L_{MO}}\right)\hat{\phi}_c\left(\frac{z-d}{l_m/\beta}\right) \tag{47}$$

The RSL function $\hat{\phi}_c$ is evaluated the same as for $\hat{\phi}_m$ using Eq. (44), but with

$$c_1 = \left[1 - \frac{S_c k}{2\beta}\phi_c^{-1}\left(\frac{h-d}{L_{MO}}\right)\right]\exp\left(c_2/2\right) \tag{48}$$

$\hat{\psi}_c$ is evaluated similar to $\hat{\psi}_m$ using Eq. (46), but with ϕ_c and $\hat{\phi}_c$.

The functions $\hat{\psi}_m$ and $\hat{\psi}_c$ must be integrated using numerical methods. In practice, however, values can be obtained from a look-up table. Eq. (46) can be expanded using Eq. (44) for $\hat{\phi}_m$ and using $l_m / \beta = 2(h-d)$ from Eq. (57) so that an equivalent equation is

$$\hat{\psi}_m\left(z\right) = c_1 \int_{z-d}^{\infty} \phi_m\left(\frac{z'}{L_{MO}}\right)\exp\left[-\frac{c_2 z'}{2(h-d)}\right]\frac{dz'}{z'} \tag{49}$$

The lower limit of integration in Eq. (49) can be rewritten as $z-d = (z-h)+(h-d)$ and dividing both sides by $h-d$ gives the expression $(z-h)/(h-d)+1$. In this notation, Eq. (49) becomes

$$\hat{\psi}_m\left(z\right) = c_1 \int_{\frac{z-h}{h-d}+1}^{\infty} \phi_m\left[\frac{(h-d)z'}{L_{MO}}\right]\exp\left(-\frac{c_2 z'}{2}\right)\frac{dz'}{z'} \tag{50}$$

In this equation, the integral is specified in a non-dimensional form and depends on two non-dimensional parameters: $(z-h)/(h-d)$ and $(h-d)/L_{MO}$. The integral is provided in a look-up table as $A[(z-h)/(h-d),(h-d)/L_{MO}]$. $\hat{\psi}_m$ is then given by $c_1 A$. A similar approach gives $\hat{\psi}_c$.

An expression for β is obtained from the relationship

$$\beta\phi_m\left(\beta^2 L_c / L_{MO}\right) = \beta_N \tag{51}$$

886 with β_N the value of $u_* / u(h)$ for neutral conditions (a representative value is $\beta_N = 0.35$, which

887 is used here). Using Eq. (39) for ϕ_m, the expanded form of Eq. (51) for unstable conditions

888 ($L_{MO} < 0$) is a quadratic equation for β^2 given by

889 $$\left(\beta^2\right)^2 + 16\frac{L_c}{L_{MO}}\beta_N^4\left(\beta^2\right) - \beta_N^4 = 0 \tag{52}$$

890 The correct solution is larger of the two roots. For stable conditions ($L_{MO} > 0$), a cubic equation

891 is obtained for β whereby

892 $$5\frac{L_c}{L_{MO}}\beta^3 + \beta - \beta_N = 0 \tag{53}$$

893 This equation has one real root. We restrict β to be in the range 0.2–0.5 (see Discussion for

894 further details).

895 The Schmidt number (S_c) is parameterized by Harman and Finnigan (2008) as

896 $$S_c = 0.5 + 0.3\tanh\left(2L_c / L_{MO}\right) \tag{54}$$

897 Eq. (21) is derived from the momentum balance equation with a first-order turbulence

898 closure in which the eddy diffusivity is specified in relation to a mixing length (l_m) that is

899 constant with height. From this, Harman and Finnigan (2007) obtained expressions for l_m and d

900 so that

901 $$l_m = 2\beta^3 L_c \tag{55}$$

902 with

903 $$L_c = \left(c_d a\right)^{-1} \tag{56}$$

904 and

905 $$h - d = \frac{l_m}{2\beta} = \beta^2 L_c \tag{57}$$

906 The term L_c is the canopy length scale (m), specified by the dimensionless leaf aerodynamic
907 drag coefficient (a common value is $c_d = 0.25$, which is used here) and plant area density (a, m^2
908 m^{-3}). For Eq. (56), plant area density is estimated as the leaf and stem area index ($L_T + S_T$)
909 divided by canopy height (h).
910
911 **A3 Obukhov length**
912 The Obukhov length is
913 $$L_{MO} = \frac{u_*^2 \theta_{vref}}{kg\theta_{v*}} \quad (58)$$
914 with θ_{vref} the virtual potential temperature (K) at the reference height, and θ_{v*} the virtual
915 potential temperature scale (K) given as
916 $$\theta_{v*} = \theta_* + 0.61\theta_{ref} q_{*kg} \quad (59)$$
917 The solution to L_{MO} requires an iterative numerical calculation (Figure 2). A value for β is
918 obtained for an initial estimate of L_{MO} using Eq. (51), which gives the displacement height (d)
919 using Eq. (57). The Schmidt number (S_c) is calculated for the current L_{MO} using Eq. (54). The
920 functions ϕ_m and ϕ_c are evaluated using Eqs. (39) and (40) at the canopy height (h) to obtain the
921 parameter c_1 as in Eqs. (45) and (48). The similarity functions ψ_m and ψ_c are evaluated at z
922 and h using Eqs. (41) and (42). The RSL functions $\hat{\psi}_m$ and $\hat{\psi}_c$ are evaluated at z and h from a
923 look-up table. u_* is obtained from Eq. (19) using the wind speed (u_{ref}) at the reference height
924 (z_{ref}). θ_* is calculated from Eq. (20) using θ_{ref} for the current timestep and $\theta(h)$ for the previous

925 sub-timestep, and a comparable equation provides q_*. A new estimate of L_{MO} is obtained, and

926 the iteration is repeated until convergence in L_{MO} is achieved.

927

928 **A4 Sparse canopies**

929 The RSL theory of Harman and Finnigan (2007, 2008) was developed for dense canopies. Sparse

930 canopies can be represented by adjusting β_N, d, and S_c for plant area index ($L_T + S_T$). The

931 neutral value for β is

932 $$\beta_N = \left[c_\beta + 0.3\left(L_T + S_T\right)\right]^{1/2} \le \beta_{N\max} \tag{60}$$

933 where

934 $$c_\beta = k^2 \left[\ln\left(\frac{h + z_{0m}}{z_{0m}} \right) \right]^{-2} \tag{61}$$

935 and z_{0m} = 0.01 m is the roughness length for momentum of the underlying ground surface. β_N

936 is constrained to be less than a maximum value for neutral conditions ($\beta_{N\max}$ = 0.35). The

937 displacement height is

938 $$h - d = \beta^2 L_c \left\{ 1 - \exp\left[-0.25\left(L_T + S_T\right) / \beta^2 \right] \right\} \tag{62}$$

939 The Schmidt number is

940 $$S_c = \left(1 - \frac{\beta_N}{\beta_{N\max}} \right) 1.0 + \frac{\beta_N}{\beta_{N\max}} \left[0.5 + 0.3 \tanh\left(2L_c / L_{MO} \right) \right] \tag{63}$$

941 This equation weights the Schmidt number between that for a neutral surface layer (1.0) and the

942 RSL value calculated from Eq. (54).

943

944 **Appendix B: List of symbols, their definition, and units**

Symbol	Description
a_i	Plant area density ($m^2\ m^{-3}$)
A_n	Leaf net assimilation (μmol $CO_2\ m^{-2}\ s^{-1}$)
c_1, c_2	Scaled magnitude (c_1) and height ($c_2 = 0.5$), respectively, for the RSL functions (–)
c_d	Leaf aerodynamic drag coefficient (0.25)
c_{dry}	Specific heat of dry biomass (1396 J $kg^{-1}\ K^{-1}$)
$c_{L,i}$	Heat capacity of leaves (J m^{-2} leaf area K^{-1})
c_p	Specific heat of air, $c_{pd}(1+0.84q_{ref.kg)})M_d$ (J $mol^{-1}\ K^{-1}$)
c_{pd}	Specific heat of dry air at constant pressure (1005 J $kg^{-1}\ K^{-1}$)
c_s	Leaf surface CO_2 concentration (μmol mol^{-1})
c_v	Soil heat capacity (J $m^{-3}\ K^{-1}$)
c_{wat}	Specific heat of water (4188 J $kg^{-1}\ K^{-1}$)
c_β	Parameter for β_N in sparse canopies (–)
d	Displacement height (m)
e_{ref}	Reference height vapor pressure (Pa)
E_i	Water vapor flux (mol $H_2O\ m^{-2}\ s^{-1}$)
E_0	Soil evaporation (mol $H_2O\ m^{-2}\ s^{-1}$)
$E_{\ell sun,i}$, $E_{\ell sha,i}$	Evaporative flux for sunlit or shaded leaves (mol $H_2O\ m^{-2}$ plant area s^{-1})
f_c	Carbon content of dry biomass (0.5 g C g^{-1})

$f_{dry,i}$	Dry transpiring fraction of canopy (–)
$f_{green,i}$	Green fraction of canopy (–)
f_i	Leaf nitrogen relative to canopy top (–)
$f_{sun,i}$	Sunlit fraction of canopy (–)
f_w	Water content of fresh biomass (0.7 g H_2O g^{-1})
$f_{wet,i}$	Wet fraction of canopy (–)
g	Gravitational acceleration (9.80665 m s^{-2})
g_0, g_1	Intercept (mol H_2O m^{-2} s^{-1}) and slope (–) for Ball–Berry stomatal conductance
$g_{a,i}$	Aerodynamic conductance (mol m^{-2} s^{-1})
$g_{b,i}$	Leaf boundary layer conductance (mol m^{-2} s^{-1})
$g_{\ell sun,i}$, $g_{\ell sha,i}$	Leaf conductance for sunlit or shaded leaves (mol H_2O m^{-2} s^{-1})
g_s	Stomatal conductance (mol H_2O m^{-2} s^{-1}); $g_{sun,i}$, sunlit leaves; $g_{sha,i}$, shaded leaves
g_{s0}	Total surface conductance for water vapor (mol H_2O m^{-2} s^{-1})
g_{soil}	Soil conductance for water vapor (mol H_2O m^{-2} s^{-1})
G_0	Soil heat flux (W m^{-2})
h	Canopy height (m)
h_s	Fractional relative humidity at the leaf surface (–)
h_{s0}	Fractional relative humidity at the soil surface (–)
H_i	Sensible heat flux (W m^{-2})

H_0	Soil sensible heat flux (W m^{-2})
$H_{\ell sun,i}$, $H_{\ell sha,i}$	Sensible heat flux for sunlit or shaded leaves (W m^{-2} plant area)
i	Canopy layer index
k	von Karman constant (0.4)
$K_{c,i}$	Scalar diffusivity (m^2 s^{-1})
K_n	Canopy nitrogen decay coefficient (–)
l_m	Mixing length for momentum (m)
L_c	Canopy length scale (m)
L_{MO}	Obukhov length (m)
L_T	Canopy leaf area index (m^2 m^{-2})
ΔL_i	Canopy layer plant area index (m^2 m^{-2})
$\Delta L_{sun,i}$, $\Delta L_{sha,i}$	Plant area index of sunlit or shaded canopy layer (m^2 m^{-2})
$\bar{M}$	Molecular mass of moist air, ρ / ρ_m (kg mol^{-1})
M_a	Leaf carbon mass per unit area (g C m^{-2} leaf area)
M_d	Molecular mass of dry air (0.02897 kg mol^{-1})
M_w	Molecular mass of water (0.01802 kg mol^{-1})
n	Time index (–)
P_{ref}	Reference height air pressure (Pa)
q_i	Water vapor concentration (mol mol^{-1})
q_0	Soil surface water vapor concentration (mol mol^{-1})

q_{ref}	Reference height water vapor concentration (mol mol^{-1})
$q_{ref.kg}$	Reference height specific humidity, $0.622e_{ref} / (P_{ref} - 0.378e_{ref})$ (kg kg^{-1})
$q_{sat}(T)$	Saturation water vapor concentration (mol mol^{-1}) at temperature T
q_*	Characteristic water vapor scale (mol mol^{-1})
$q_{*.kg}$	Characteristic water vapor scale, $q_* M_w / \bar{M}$ (kg kg^{-1})
R_{n0}	Soil surface net radiation (W m^{-2})
$R_{n\ell sun,i}$, $R_{n\ell sha,i}$	Net radiation for sunlit or shaded leaves (W m^{-2} plant area)
$\Re$	Universal gas constant (8.31446 J K^{-1} mol^{-1})
s_i^{sun}, s_i^{sha}	Temperature derivative of saturation water vapor concentration evaluated at $T_{\ell sun,i}$ and $T_{\ell sha,i}$, dq_{sat}/dT (mol mol^{-1} K^{-1})
s_0	Temperature derivative of saturation water vapor concentration evaluated at the soil surface temperature T_0, dq_{sat}/dT (mol mol^{-1} K^{-1})
S_c	Schmidt number at the canopy top (–)
S_T	Canopy stem area index (m^2 m^{-2})
t	Time (s)
T_0	Soil surface temperature (K)
$T_{\ell sun,i}$, $T_{\ell sha,i}$	Temperature of sunlit or shaded leaves (K)
T_{ref}	Reference height temperature (K)
T_{soil}	Temperature of first soil layer (K)
u_i	Wind speed (m s^{-1})

u_{ref}	Reference height wind speed (m s^{-1})
u_*	Friction velocity (m s^{-1})
$V_{c\max}$	Maximum carboxylation rate (μmol m^{-2} s^{-1})
W_i	Intercepted water (kg H_2O m^{-2})
z_i	Height (m)
z_{ref}	Reference height (m)
$z_{0m,g}$, $z_{0c,g}$	Roughness length of ground for momentum (0.01 m) and scalars (0.001 m), respectively
Δz_{soil}	Depth of first soil layer (m)
β	Ratio of friction velocity to wind speed at the canopy height (–)
β_N	Neutral value of β (0.35)
$\beta_{N\max}$	Maximum value of β_N in a sparse canopy (0.35)
ζ	Monin–Obukhov dimensionless parameter (–)
θ_i	Potential temperature (K)
θ_{ref}	Reference height potential temperature (K)
θ_s	Aerodynamic surface temperature (K)
θ_{vref}	Reference height virtual potential temperature (K)
θ_{v*}	Characteristic virtual potential temperature scale (K)
θ_*	Characteristic potential temperature scale (K)
ι	Marginal water-use efficiency parameter (μmol CO_2 mol^{-1} H_2O)
κ_{soil}	Thermal conductivity of first soil layer (W m^{-1} K^{-1})

ξ	RSL dimensionless parameter (–)
λ	Latent heat of vaporization (45.06802 kJ mol^{-1})
ρ	Density of moist air, $\rho_m M_d (1-0.378 e_{ref} / P_{ref})$ (mol m^{-3})
ρ_m	Molar density, $P_{ref} / \Re T_{ref}$ (mol m^{-3})
ϕ_m, ϕ_c	Monin–Obukhov similarity theory flux–gradient relationships for momentum and scalars (–)
$\hat{\phi}_m$, $\hat{\phi}_c$	RSL modification of flux–gradient relationships for momentum and scalars (–)
Φ_m, Φ_c	RSL-modified flux–gradient relationships for momentum and scalars (–)
ψ_ℓ, $\psi_{\ell \min}$	Leaf water potential and its minimum value (MPa)
ψ_m, ψ_c	Integrated form of Monin–Obukhov stability functions for momentum and scalars (–)
$\hat{\psi}_m$, $\hat{\psi}_c$	Integrated form of the RSL stability functions for momentum and scalars (–)

The Supplement related to this article is available online.

Author contributions. E. Patton, I. Harman, and J. Finnigan developed the RSL code. G. Bonan developed the numerical solution for scalar profiles in the canopy. G. Bonan and E. Patton implemented the code in the multi-layer canopy. G. Bonan and E. Patton designed the model simulations. K. Oleson performed the CLM4.5 simulations. Y. Lu provided the US-ARM data, and E. Burakowski processed the US-Dk1, US-Dk2, and US-Dk3 data. G. Bonan wrote the manuscript with contributions from all co-authors.

Competing interests. The authors declare that they have no conflict of interest.

Acknowledgments. The National Center for Atmospheric Research is sponsored by the National Science Foundation. This work was supported by the National Science Foundation Science and Technology Center for Multi-Scale Modeling of Atmospheric Processes, managed by Colorado State University under cooperative agreement No. ATM-0425247.

References

Alkama, R., and Cescatti, A.: Biophysical climate impacts of recent changes in global forest cover, Science, 351, 600–604, 2016.

Ashworth, K., Chung, S. H., Griffin, R. J., Chen, J., Forkel, R., Bryan, A. M., and Steiner, A. L.: FORest Canopy Atmosphere Transfer (FORCAsT) 1.0: A 1-D model of biosphere–atmosphere chemical exchange, Geosci. Model Dev., 8, 3765–3784, 2015.

Ball, M. C., Cowan, I. R., and Farquhar, G. D.: Maintenance of leaf temperature and the optimisation of carbon gain in relation to water loss in a tropical mangrove forest, Aust. J. Plant Physiol., 15, 263–276, 1988.

Blanken, P. D., Black, T. A., Yang, P. C., Neumann, H. H., Nesic, Z., Staebler, R., den Hartog, G., Novak, M. D., and Lee, X.: Energy balance and canopy conductance of a boreal aspen forest: partitioning overstory and understory components, J. Geophys. Res, 102D, 28915–28927, 1997.

Bonan, G. B.: A Land Surface Model (LSM Version 1.0) for Ecological, Hydrological, and Atmospheric Studies: Technical Description and User's Guide, NCAR Tech. Note

977 NCAR/TN-417+STR, National Center for Atmospheric Research, Boulder, Colorado,
978 1996.
979 Bonan, G. B., Williams, M., Fisher, R. A., and Oleson, K. W.: Modeling stomatal conductance in
980 the earth system: linking leaf water-use efficiency and water transport along the soil–
981 plant–atmosphere continuum, Geosci. Model Dev., 7, 2193–2222, 2014.
982 Brutsaert, W.: Evaporation into the Atmosphere: Theory, History, and Applications, Kluwer,
983 Dordrecht, 1982.
984 Burakowski, E., Tawfik, A., Ouimette, A., Lepine, L., Novick, K., Ollinger, S., Zarzycki, C., and
985 Bonan, G.: The role of surface roughness, albedo, and Bowen ratio on ecosystem energy
986 balance in the Eastern United States, Agr. For. Meteorol., 249, 367–367, 2018.
987 Chen, Y., Ryder, J., Bastrikov, V., McGrath, M. J., Naudts, K., Otto, J., Ottlé, C., Peylin, P.,
988 Polcher, J., Valade, A., Black, A., Elbers, J. A., Moors, E., Foken, T., van Gorsel, E.,
989 Haverd, V., Heinesch, B., Tiedemann, F., Knohl, A., Launiainen, S., Loustau, D., Ogée,
990 J., Vesala, T., and Luyssaert, S.: Evaluating the performance of land surface model
991 ORCHIDEE-CAN v1.0 on water and energy flux estimation with a single- and multi-
992 layer energy budget scheme, Geosci. Model Dev., 9, 2951–2972, 2016.
993 Choudhury, B. J. and Monteith, J. L.: A four-layer model for the heat budget of homogeneous
994 land surfaces, Q. J. Roy. Meteor. Soc., 114, 373–398, 1988.
995 Cionco, R. M.: A mathematical model for air flow in a vegetative canopy, J. Appl. Meteorol., 4,
996 517–522, 1965.
997 Cionco, R. M.: Analysis of canopy index values for various canopy densities, Bound.-Lay.
998 Meteorol., 15, 81–93, 1978.

Clark, M. P., Nijssen, B., Lundquist, J. D., Kavetski, D., Rupp, D. E., Woods, R. A., Freer, J. E., Gutmann, E. D., Wood, A. W., Gochis, D. J., Rasmussen, R. M., Tarboton, D. G., Mahat, V., Flerchinger, G. N., and Marks, D. G.: A unified approach for process-based hydrologic modeling: 2. Model implementation and case studies, Water Resour. Res., 51, 2515–2542, doi:10.1002/2015WR017200, 2015.

Dai, Y., Dickinson, R. E., and Wang, Y.-P.: A two-big-leaf model for canopy temperature, photosynthesis, and stomatal conductance, J. Climate, 17, 2281–2299, 2004.

Deardorff, J. W.: Efficient prediction of ground surface temperature and moisture, with inclusion of a layer of vegetation, J. Geophys. Res., 83C, 1889–1903, 1978.

De Frenne, P., Rodríguez-Sánchez, F., Coomes, D. A., Baeten, L., Verstraeten, G., Vellend, M., Bernhardt-Römermann, M., Brown, C. D., Brunet, J., Cornelis, J., Decocq, G. M., Dierschke, H., Eriksson, O., Gilliam, F. S., Hédl, R., Heinken, T., Hermy, M., Hommel, P., Jenkins, M. A., Kelly, D. L., Kirby, K. J., Mitchell, F. J. G., Naaf, T., Newman, M., Peterken, G., Petřík, P., Schultz, J., Sonnier, G., Van Calster, H., Waller, D. M., Walther, G.-R., White, P. S., Woods, K. D., Wulf, M., Graae, B. J., and Verheyen, K.: Microclimate moderates plant responses to macroclimate warming, Proc. Natl. Acad. Sci. U.S.A, 110, 18561–18565, 2013.

Dickinson, R. E., Henderson-Sellers, A., Kennedy, P. J., and Wilson, M. F.: Biosphere–Atmosphere Transfer Scheme (BATS) for the NCAR Community Climate Model, NCAR Tech. Note NCAR/TN-275+STR, National Center for Atmospheric Research, Boulder, Colorado, 1986.

Dolman, A. J.: A multiple-source land surface energy balance model for use in general circulation models, Agr. For. Meteorol., 65, 21–45, 1993.

1022 Finnigan J. J. and Raupach M. R.: Transfer processes in plant canopies in relation to stomatal
1023 characteristics, in: Stomatal Function, edited by: Zeiger, E., Farquhar, G. D., and Cowan,
1024 I. R., Stanford University Press, Stanford, Calif., 385–429, 1987.
1025 Finnigan, J. J., Shaw, R. H., and Patton, E. G.: Turbulence structure above a vegetation canopy,
1026 J. Fluid Mech., 637, 387–424, 2009.
1027 Foken, T.: 50 years of the Monin–Obukhov similarity theory, Bound.-Lay. Meteorol., 119, 431–
1028 447, 2006.
1029 Forkel, R., Klemm, O., Graus, M., Rappenglück, B., Stockwell, W. R., Grabmer, W., Held, A.,
1030 Hansel, A., and Steinbrecher, R.: Trace gas exchange and gas phase chemistry in a
1031 Norway spruce forest: A study with a coupled 1-dimensional canopy atmospheric
1032 chemistry emission model, Atmos. Environ., 40, S28–S42, 2006.
1033 Franks, P. J., Berry, J. A., Lombardozzi, D. L., and Bonan, G. B.: Stomatal function across
1034 temporal and spatial scales: deep-time trends, land-atmosphere coupling and global
1035 models, Plant Physiology, 174, 583–602, 2017.
1036 Friedlingstein, P., Cox, P., Betts, R., Bopp, L., von Bloh, W., Brovkin, V., Cadule, P., Doney, S.,
1037 Eby, M., Fung, I., Bala, G., John, J., Jones, C., Joos, F., Kato, T., Kawamiya, M., Knorr,
1038 W., Lindsay, K., Matthews, H. D., Raddatz, T., Rayner, P., Reick, C., Roeckner, E.,
1039 Schnitzler, K.-G., Schnur, R., Stassmann, K., Weaver, A. J., Yoshikawa, C., and Zeng,
1040 N.: Climate–carbon cycle feedback analysis: results from the C^4MIP model
1041 intercomparison, J. Climate, 19, 3337–3353, 2006.
1042 Friedlingstein, P., Meinshausen, M., Arora, V. K., Jones, C. D., Anav, A., Liddicoat, S. K., and
1043 Knutti, R.: Uncertainties in CMIP5 climate projections due to carbon cycle feedbacks, J.
1044 Climate, 27, 511–526, 2014.

1045 Garratt, J. R.: Flux profile relations above tall vegetation, Q. J. Roy. Meteor. Soc., 104, 199–
1046 211, 1978.
1047 Geiger, R.: Das Klima der bodennahen Luftschicht, Friedr. Vieweg & Sohn, Braunschweig,
1048 Germany, 1927.
1049 Harman, I. N.: The role of roughness sublayer dynamics within surface exchange schemes,
1050 Bound.-Lay. Meteorol., 142, 1–20, 2012.
1051 Harman, I. N. and Finnigan, J. J.: A simple unified theory for flow in the canopy and roughness
1052 sublayer, Bound.-Lay. Meteorol., 123, 339–363, 2007.
1053 Harman, I. N. and Finnigan, J. J.: Scalar concentration profiles in the canopy and roughness
1054 sublayer, Bound.-Lay. Meteorol., 129, 323–351, 2008.
1055 Haverd, V., Leuning, R., Griffith, D., van Gorsel, E., and Cuntz, M.: The turbulent Lagrangian
1056 time scale in forest canopies constrained by fluxes, concentrations and source
1057 distributions, Bound.-Lay. Meteorol., 130, 209–228, 2009.
1058 Hollinger, S. E., Bernacchi, C. J., and Meyers, T. P.: Carbon budget of mature no-till ecosystem
1059 in North Central Region of the United States, Agr. For. Meteorol., 130, 59–69, 2005.
1060 Inoue, E.: On the turbulent structure of airflow within crop canopies, J. Meteorol. Soc. Japan Ser.
1061 II, 41, 317–326, 1963.
1062 Jarvis, P. G. and McNaughton, K. G.: Stomatal control of transpiration: scaling up from leaf to
1063 region, Adv. Ecol. Res., 15, 1–49, 1986.
1064 Juang, J.-Y., Katul, G. G., Siqueira, M. B., Stoy, P. C., and McCarthy, H. R.: Investigating a
1065 hierarchy of Eulerian closure models for scalar transfer inside forested canopies, Bound.-
1066 Lay. Meteorol, 128, 1–32 (2008).
1067 Kucharik, C. J. and Twine, T. E.: Residue, respiration, and residuals: evaluation of a dynamic

agroecosystem model using eddy flux measurements and biometric data, Agr. For. Meteorol., 146, 134–158, 2007.

Kucharik, C. J., Norman, J. M., and Gower, S. T.: Measurements of branch area and adjusting leaf area index indirect measurements, Agr. For. Meteorol., 91, 69–88, 1998.

Levis, S., Bonan, G. B., Kluzek, E., Thornton, P. E., Jones, A., Sacks, W. J., and Kucharik, C. J.: Interactive crop management in the Community Earth System Model (CESM1): seasonal influences on land-atmosphere fluxes, J. Climate, 25, 4839–4859, 2012.

Lu, Y., Williams, I. N., Bagley, J. E., Torn, M. S., and Kueppers, L. M.: Representing winter wheat in the Community Land Model (version 4.5), Geosci. Model Dev., 10, 1873–1888, 2017.

Mahat, V., Tarboton, D. G., and Molotch, N. P.: Testing above- and below-canopy representations of turbulent fluxes in an energy balance snowmelt model, Water Resour. Res., 49, doi:10.1002/wrcr.20073, 2013.

Massman, W. J.: An analytical one-dimensional model of momentum transfer by vegetation of arbitrary structure, Bound.-Lay. Meteorol., 83, 407–421, 1997.

Massman, W. J. and Weil, J. C.: An analytical one-dimensional second-order closure model of turbulence statistics and the Lagrangian time scale within and above plant canopies of arbitrary structure, Bound.-Lay. Meteorol., 91, 81–107, 1999.

McNaughton, K. G. and van den Hurk, B. J. J. M.: A 'Lagrangian' revision of the resistors in the two-layer model for calculating the energy budget of a plant canopy, Bound.-Lay. Meteorol., 74, 261–288, 1995.

Meyers, T. P. and Hollinger, S. E.: An assessment of storage terms in the surface energy balance of maize and soybean, Agr. For. Meteorol., 125, 105–115, 2004.

1091 Meyers, T. P., Finkelstein, P., Clarke, J., Ellestad, T. G., and Sims, P. F.: A multilayer model for
1092 inferring dry deposition using standard meteorological measurements, J. Geophys. Res.,
1093 103D, 22645–22661, 1998.
1094 Niinemets, Ü.: Components of leaf dry mass per area – thickness and density – alter leaf
1095 photosynthetic capacity in reverse directions in woody plants, New Phytol., 144, 35–47,
1096 1999.
1097 Niu, G.-Y. and Yang, Z.-L.: Effects of vegetation canopy processes on snow surface energy and
1098 mass balances, J. Geophys. Res., 109, D23111, doi:10.1029/2004JD004884, 2004.
1099 Norman, J. M.: Modeling the complete crop canopy, in: Modification of the Aerial Environment
1100 of Plants, edited by: Barfield, B. J. and Gerber, J. F., Am. Soc. of Agric. Eng., St. Joseph,
1101 Mich, 249–277, 1979.
1102 Norman, J. M. and Jarvis, P. G.: Photosynthesis in Sitka spruce (*Picea sitchensis* (Bong.) Carr.).
1103 III. Measurements of canopy structure and interception of radiation, J. Appl. Ecol., 11,
1104 375–398, 1974.
1105 Novick, K. A., Stoy, P. C., Katul, G. G., Ellsworth, D. S., Siqueira, M. B. S., Juang, J., and Oren,
1106 R.: Carbon dioxide and water vapor exchange in a warm temperate grassland, Oecologia,
1107 138, 259–274, 2004.
1108 Oleson, K.W., Lawrence, D. M., Bonan, G. B., Drewniak, B., Huang, M., Koven, C. D., Levis,
1109 S., Li, F., Riley, W. J., Subin, Z. M., Swenson, S. C., Thornton, P. E., Bozbiyik, A.,
1110 Fisher, R., Heald, C. L., Kluzek, E., Lamarque, J.-F., Lawrence, P. J., Leung, L. R.,
1111 Lipscomb, W., Muszala, S., Ricciuto, D. M., Sacks, W., Sun, Y., Tang, J. and Yang, Z.-
1112 L.: Technical description of version 4.5 of the Community Land Model (CLM), NCAR

1113 Tech. Note NCAR/TN-503+STR, National Center for Atmospheric Research, Boulder,
1114 Colorado, 2013.
1115 Patton, E. G., Horst, T. W., Sullivan, P. P., Lenschow, D. H., Oncley, S. P., Brown, W. O.,
1116 Burns, S. P., Guenther, A. B., Held, A., Karl, T., Mayor, S. D., Rizzo, L. V., Spuler, S.
1117 M., Sun, J., Turnipseed, A. A., Allwine, E. J., Edburg, S. L., Lamb, B. K., Avissar, R.,
1118 Calhoun, R. J., Kleissl, J., Massman, W. J., Paw U, K. T., and Weil, J. C.: The Canopy
1119 Horizontal Array Turbulence Study. Bull. Amer. Meteor. Soc., 92, 593–611, 2011.
1120 Physick, W. L. and Garratt, J. R.: Incorporation of a high-roughness lower boundary into a
1121 mesoscale model for studies of dry deposition over complex terrain, Bound.-Lay.
1122 Meteorol., 74, 55–71, 1995.
1123 Pyles, R. D., Weare, B. C., and Paw U, K. T.: The UCD Advanced Canopy–Atmosphere–Soil
1124 Algorithm: comparisons with observations from different climate and vegetation regimes,
1125 Q. J. Roy. Meteor. Soc., 126, 2951–2980, 2000.
1126 Raupach, M. R.: Simplified expressions for vegetation roughness length and zero-plane
1127 displacement as functions of canopy height and area index, Bound.-Lay. Meteorol., 71,
1128 211–216, 1994.
1129 Raupach, M. R.: A practical Lagrangian method for relating scalar concentrations to source
1130 distributions in vegetation canopies, Q. J. Roy. Meteor. Soc., 115, 609–632, 1989.
1131 Raupach, M. R., Finnigan, J. J., and Brunet, Y.: Coherent eddies and turbulence in vegetation
1132 canopies: the mixing-length analogy, Bound.-Lay. Meteorol., 78, 351–382, 1996.
1133 Raupach, M. R., Finkele, K., and Zhang, L.: SCAM (Soil-Canopy-Atmosphere Model):
1134 Description and Comparisons with Field Data, Tech. Rep. No. 132, CSIRO Centre for
1135 Environmental Mechanics, Canberra, Australia, 1997.

1136 Richardson, A. D., Hollinger, D. Y., Burba, G. G., Davis, K. J., Flanagan, L. B., Katul, G. G.,
1137 Munger, J. W., Ricciuto, D. M., Stoy, P. C., Suyker, A. E., Verma, S. B. and Wofsy, S.
1138 C.: A multi-site analysis of random error in tower-based measurements of carbon and
1139 energy fluxes, Agric. For. Meteorol., 136, 1–18, 2006.
1140 Richardson, A. D., Aubinet, M., Barr, A. G., Hollinger, D. Y., Ibrom, A., Lasslop, G., and
1141 Reichstein, M.: Uncertainty quantification, in: Eddy Covariance: A Practical Guide to
1142 Measurement and Data Analysis, edited by: Aubinet, M., Vesala, T. and Papale, D.,
1143 Springer, Dordrecht, 173–209, 2012.
1144 Richtmyer, R. D. and Morton, K. W.: Difference Methods for Initial-Value Problems, 2nd ed.,
1145 Wiley, New York, 1967.
1146 Ryder, J., Polcher, J., Peylin, P., Ottlé, C., Chen, Y., van Gorsel, E., Haverd, V., McGrath, M. J.,
1147 Naudts, K., Otto, J., Valade, A., and Luyssaert, S.: A multi-layer land surface energy
1148 budget model for implicit coupling with global atmospheric simulations, Geosci. Model
1149 Dev., 9, 223–245, 2016.
1150 Ryu, Y., Baldocchi, D. D., Ma, S., and Hehn, T.: Interannual variability of evapotranspiration
1151 and energy exchange over an annual grassland in California, J. Geophys. Res., 113,
1152 D09104, doi:10.1029/2007JD009263, 2008.
1153 Schaefer, K., Schwalm, C. R., Williams, C., Arain, M. A., Barr, A., Chen, J. M., Davis, K. J.,
1154 Dimitrov, D., Hilton, T. W., Hollinger, D. Y., Humphreys, E., Poulter, B., Raczka, B. M.,
1155 Richardson, A. D., Sahoo, A., Thornton, P., Vargas, R., Verbeeck, H., Anderson, R.,
1156 Baker, I., Black, T. A., Bolstad, P., Chen, J., Curtis, P. S., Desai, A. R., Dietze, M.,
1157 Dragoni, D., Gough, C., Grant, R. F., Gu, L., Jain, A., Kucharik, C., Law, B., Liu, S.,
1158 Lokipitiya, E., Margolis, H. A., Matamala, R., McCaughey, J. H., Monson, R., Munger, J.

W., Oechel, W., Peng, C., Price, D. T., Ricciuto, D., Riley, W. J., Roulet, N., Tian, H., Tonitto, C., Torn, M., Weng, E., and Zhou, X.: A model–data comparison of gross primary productivity: results from the North American Carbon Program site synthesis, J. Geophys. Res., 117, G03010, doi:10.1029/2012JG001960, 2012.

Scheffers, B. R., Phillips, B. L., Laurance, W. F., Sodhi, N. S., Diesmos, A., and Williams, S. E.: Increasing arboreality with altitude: a novel biogeographic dimension, Proc. R. Soc. B, 280, 20131581, doi:10.1098/rspb.2013.1581, 2013.

Sellers, P. J., Mintz, Y., Sud, Y. C., and Dalcher, A.: A simple biosphere model (SiB) for use within general circulation models, J. Atmos. Sci., 43, 505–531, 1986.

Sellers, P. J., Randall, D. A., Collatz, G. J., Berry, J. A., Field, C. B., Dazlich, D. A., Zhang, C., Collelo, G. D., and Bounoua, L.: A revised land surface parameterization (SiB2) for atmospheric GCMs. Part I: Model formulation, J. Climate, 9, 676–705, 1996.

Shapkalijevski, M., Moene, A. F., Ouwersloot, H. G., Patton, E. G., and Vilà-Guerau de Arellano, J.: Influence of canopy seasonal changes on turbulence parameterization within the roughness sublayer over an orchard canopy, J. Appl. Meteor. Climatol., 55, 1391–1407, 2016.

Shaw, R. H. and Pereira, A. R.: Aerodynamic roughness of a plant canopy: a numerical experiment, Agr. Meteorol., 26, 51–65, 1982.

Shuttleworth, W. J. and Wallace, J. S.: Evaporation from sparse crops – an energy combination theory, Q. J. Roy. Meteor. Soc., 111, 839–855, 1985.

Siqueira, M., Leuning, R., Kolle, O., Kelliher, F. M., and Katul, G. G.: Modelling sources and sinks of CO_2, H_2O and heat within a Siberian pine forest using three inverse methods, Q. J. Roy. Meteor. Soc., 129, 1373–1393, 2003.

Staudt, K., Serafimovich, A., Siebicke, L., Pyles, R. D., and Falge, E.: Vertical structure of evapotranspiration at a forest site (a case study), Agr. For. Meteorol., 151, 709–729, 2011.

Stoy, P. C., Katul, G. G., Siqueira, M. B. S., Juang, J.-Y., Novick, K. A., McCarthy, H. R., Oishi, A. C., Uebelherr, J. M., Kim, H.-S., and Oren, R.: Separating the effects of climate and vegetation on evapotranspiration along a successional chronosequence in the southeastern US, Global Change Biol., 12, 2115–2135, 2006.

Stroud, C., Makar, P., Karl, T., Guenther, A., Geron, C., Turnipseed, A., Nemitz, E., Baker, B., Potosnak, M., and Fuentes, J. D.: Role of canopy-scale photochemistry in modifying biogenic-atmosphere exchange of reactive terpene species: Results from the CELTIC field study, J. Geophys. Res., 110, D17303, doi:10.1029/2005JD005775, 2005.

Taylor, K. E.: Summarizing multiple aspects of model performance in a single diagram, J. Geophys. Res., 106D, 7183–7192, 2001.

Thom, A. S.: Momentum, mass and heat exchange of plant communities, in: Vegetation and the Atmosphere: vol. 1. Principles, edited by: Monteith, J. L., Academic Press, New York, 57–109, 1975.

Verma, S. B., Dobermann, A., Cassman, K. G., Walters, D. T., Knops, J. M., Arkebauer, T. J., Suyker, A. E., Burba, G. G., Amos, B., Yang, H., Ginting, D., Hubbard, K. G., Gitelson, A. A., and Walter-Shea, E. A.: Annual carbon dioxide exchange in irrigated and rainfed maize-based agroecosystems, Agr. For. Meteorol., 131, 77–96, 2005.

Wang, Y.-P. and Leuning, R.: A two-leaf model for canopy conductance, photosynthesis and partitioning of available energy. I: Model description and comparison with a multi-layered model, Agr. For. Meteorol., 91, 89–111, 1998.

Williams, M., Rastetter, E. B., Fernandes, D. N., Goulden, M. L., Wofsy, S. C., Shaver, G. R., Melillo, J. M., Munger, J. W., Fan, S.-M., and Nadelhoffer, K. J.: Modelling the soil–plant–atmosphere continuum in a *Quercus–Acer* stand at Harvard Forest: the regulation of stomatal conductance by light, nitrogen and soil/plant hydraulic properties, Plant Cell Environ., 19, 911–927, 1996.

Wolfe, G. M. and Thornton, J. A.: The Chemistry of Atmosphere–Forest Exchange (CAFE) model – Part 1: Model description and characterization, Atmos. Chem. Phys., 11, 77–101 (2011).

Wu, Y., Brashers, B., Finkelstein, P. L., and Pleim, J. E.: A multilayer biochemical dry deposition model. 1. Model formulation, J. Geophys. Res., 108D, 4013, doi:10.1029/2002JD002293, 2003.

Zeng, X., Barlage, M., Dickinson, R.E., Dai, Y., Wang, G., and Oleson, K.: Treatment of undercanopy turbulence in land models, J. Climate, 18, 5086–5094, 2005.

Table 1. Leaf heat capacity

Plant functional type	Specific leaf area (m^2 g^{-1} C)	Leaf mass per area (g dry mass m^{-2})	Heat capacity (J m^{-2} K^{-1})
Grass, crop	0.03	67	745
Deciduous broadleaf tree	0.03	67	745
Evergreen needleleaf tree			
Temperate	0.01	200	2234
Boreal	0.008	250	2792

Table 2. Site information for the 4 deciduous broadleaf forest (DBF), 3 evergreen needleleaf forest (ENF), 2 grassland (GRA), and 3 cropland (CRO) flux towers, including mean temperature (T) and precipitation (P) for the simulation month.

Site	Vegetation type	Latitude	Longitude	T (°C)	P (mm)	Years	Month	Leaf area index[a]	Canopy height (m)
US-Dk2	DBF	35.97	–79.10	24.7	128	2004–2008	July	6.2	25
US-Ha1	DBF	42.54	–72.17	20.0	103	1992–2006	July	4.9	23
US-MMS	DBF	39.32	–86.41	24.1	112	1999–2006	July	4.7	27
US-UMB	DBF	45.56	–84.71	20.2	63	1999–2006	July	4.2	21
US-Dk3	ENF	35.98	–79.09	24.6	126	2004–2008	July	4.7	17
US-Ho1	ENF	45.20	–68.74	19.3	77	1996–2004	July	4.6	20
US-Me2	ENF	44.45	–121.56	19.1	4	2002–2007	July	3.8	14
US-Dk1[b]	GRA	35.97	–79.09	25.1	128	2004–2008	July	1.7	0.5

Deleted: annual
Deleted: MA
Deleted: annual
Deleted: rec

US-Var	GRA	38.41	–120.95	12.3	80	2001–2007	March	2.4	0.6
US-ARM	CRO	36.61	–97.49	14.7	98	2003–4, 2006–7, 2009–10	April	2–4	0.5
US-Bo1	CRO	40.01	–88.29	22.3	53	1998–2006 (even)	August	5.0	0.9
US-Ne3	CRO	41.18	–96.44	21.8	111	2002, 2004	August	3.7	0.9

[a] Shown is the maximum for the month. Maximum leaf area index for US-ARM varied by year, and shown is the range in monthly maximum across all years.

[b] H and u_* for 2007 and 2008 are excluded.

1245 Table 3. Major differences between the CLM4.5 and ML+RSL

Feature	CLM4.5	ML+RSL
Canopy	Dual source: vegetation (sunlit/shaded big-leaf) and soil	Multilayer; sunlit and shaded leaf fluxes at each level; scalar profiles (u, θ, q) based on conservation equations
Plant area index	Big leaf	Vertical profile uses beta distribution probability density function for leaves and uniform profile for stems
Stomatal conductance	$g_s = g_0 + g_1 h_s A_n / c_s$	$\Delta A_n / \Delta E_\ell = \iota$ with $\psi_\ell > \psi_{\ell\min}$; Bonan et al. (2014)
Relative leaf nitrogen profile $f_i = \exp[-K_n \sum \Delta L_j]$	$K_n = 0.3$	$K_n = \exp(0.00963 V_{c\max} - 2.43)$; Bonan et al. (2014)
Storage	–	Plant: $c_L(\Delta T_\ell / \Delta t)$ Air: $\rho_m c_p \Delta z(\Delta\theta / \Delta t)$ Air: $\rho_m \Delta z(\Delta q / \Delta t)$
Above-canopy turbulence	MOST	RSL
Within-canopy turbulence	Understory wind speed equals u_*; aerodynamic conductance based on u_* and understory Ri.	$u(z) = u(h)\exp\left[(z-h)\beta / l_m\right]$ $K_c(z) = K_c(h)\exp\left[(z-h)\beta / l_m\right]$

1246 Table 4. Summary of simulation changes to the turbulence parameterization and leaf biophysics

Simulation	Turbulence		Biophysical			
	θ, q	u, g_a	g_s	K_n	Plant area density	c_L
CLM4.5	CLM4.5	CLM4.5	CLM4.5	CLM4.5	$(L_T + S_T)/h$	–
m0	Well-mixed	–	″	″	″	″
m1	Eqs. (16) and (17)	$z > h$: CLM4.5 $z < h$: Eqs. (21) and (26), $\eta = 3$	″	″	″	″
b1	″	″	Bonan et al. (2014)	″	″	″
b2	″	″	″	Bonan et al. (2014)	″	″
b3	″	″	″	″	Eq. (28)	″
b4	″	″	″	″	″	Eq. (29)
r1	″	$z > h$: Eqs. (19) and (24) $z < h$: Eqs. (21) and (26), $\eta = 3$	″	″	″	″
r2	″	″, but with l_m / β	″	″	″	″

1247

Table 5. Average Taylor skill score for the ML+RSL (first number) and CLM4.5 (second number) simulations. Skill scores greater than those of CLM4.5 are highlighted in bold.

Site	R_n	H	λE	u_*	T_{rad}	GPP
Forest						
US-Ha1	**0.98**/0.98	**0.89**/0.85	**0.94**/0.92	**0.91**/0.82	–	**0.83**/0.80
US-MMS	**1.00**/0.99	0.44/0.47	**0.88**/0.87	**0.84**/0.78	**0.89**/0.81	0.70/0.70
US-UMB	0.99/0.99	**0.90**/0.84	**0.92**/0.88	**0.93**/0.89	**0.92**/0.75	**0.81**/0.73
US-Dk2	**0.98**/0.98	**0.53**/0.52	0.93/0.93	**0.86**/0.82	**0.75**/0.75	–
US-Dk3	**0.99**/0.99	**0.85**/0.85	0.94/0.94	0.81/0.82	**0.83**/0.79	–
US-Ho1	0.96/0.97	0.93/0.94	0.91/0.93	**0.92**/0.86	–	0.86/0.87
US-Me2	**1.00**/1.00	**0.90**/0.79	**0.89**/0.64	**0.88**/0.84	**0.94**/0.78	**0.91**/0.57
Herbaceous						
US-Dk1	0.99/0.99	**0.89**/0.87	0.90/0.90	0.73/0.82	**0.98**/0.95	–
US-Var	0.95/0.96	**0.72**/0.59	**0.95**/0.95	**0.81**/0.79	0.98/0.98	**0.89**/0.79
US-Bo1	0.99/0.99	**0.75**/0.61	**0.96**/0.94	**0.94**/0.94	**0.90**/0.85	–
US-Ne3	**1.00**/1.00	**0.48**/0.35	**0.85**/0.77	**0.98**/0.96	**0.94**/0.86	**0.78**/0.59
US-ARM	0.96/0.97	**0.93**/0.88	0.91/0.94	0.95/0.95	**0.98**/0.97	–

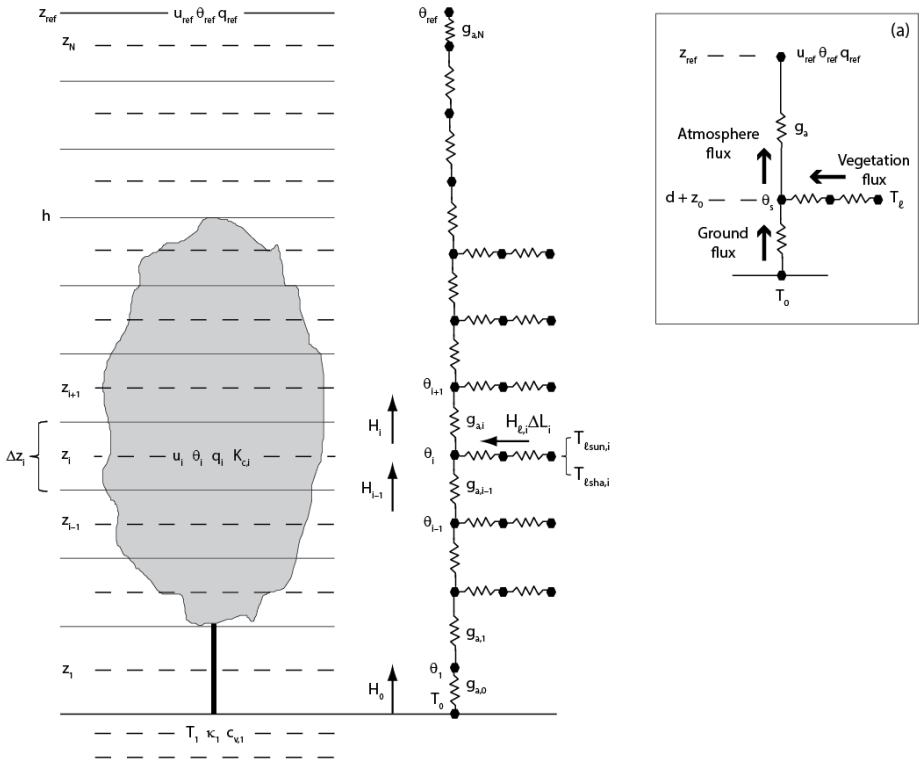

Figure 1. Numerical grid used to represent a multi-layer canopy. The volume of air from the reference height (z_{ref}) to the ground consists of N layers with a thickness Δz_i, plant area index ΔL_i, and plant area density $a_i = \Delta L_i / \Delta z_i$. The canopy has a height h. Wind speed (u_i), temperature (θ_i), water vapor concentration (q_i), and scalar diffusivity ($K_{c,i}$) are physically centered in each layer at height z_i. An aerodynamic conductance ($g_{a,i}$) regulates the turbulent flux between layer i to $i+1$. The right-hand side of the figure depicts the sensible heat fluxes below and above layer i (H_{i-1} and H_i) and the total vegetation source/sink flux ($H_{\ell,i}\Delta L_i$) with

sunlit and shaded components. Shown is the conductance network, in which nodal points represent scalar values in the air and at the leaf. Canopy source/sink fluxes depend on leaf conductances and leaf temperature, calculated separately for sunlit and shaded leaves using the temperatures $T_{\ell sun,i}$ and $T_{\ell sha,i}$, respectively. The ground is an additional source/sink of heat and water vapor with temperature T_0. The inset panel (a) shows the dual-source canopy model used in the Community Land Model (CLM4.5). Here, Monin–Obukhov similarity theory provides the flux from the surface with height $d + z_0$ (displacement height d plus roughness length z_0) and temperature θ_s to the reference height with the conductance g_a. In the CLM4.5, d and z_0 are prescribed fractions of canopy height.

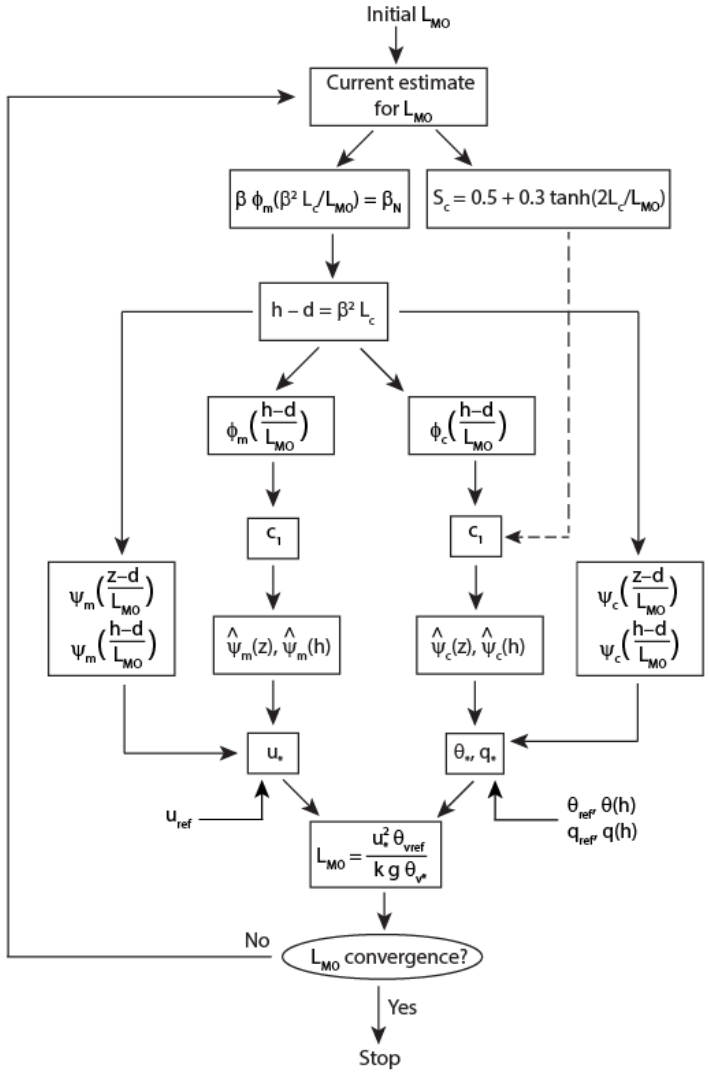

Figure 2. Flow diagram for calculating the Obukhov length (L_{MO}).

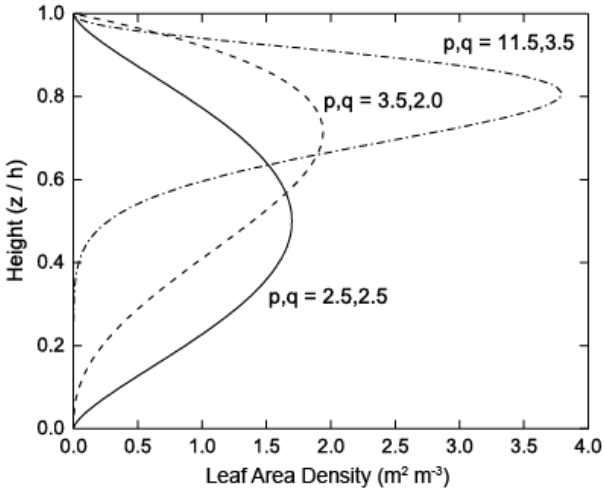

Figure 3. Profiles of leaf area density. Shown are three different canopy profiles for: (i) grass and crop with $p = q = 2.5$; (ii) deciduous and spruce trees with $p = 3.5$ and $q = 2.0$; and (iii) pine trees with $p = 11.5$ and $q = 3.5$. These profiles are show here with $L_T / h = 0.5$ m^2 m^{-3}.

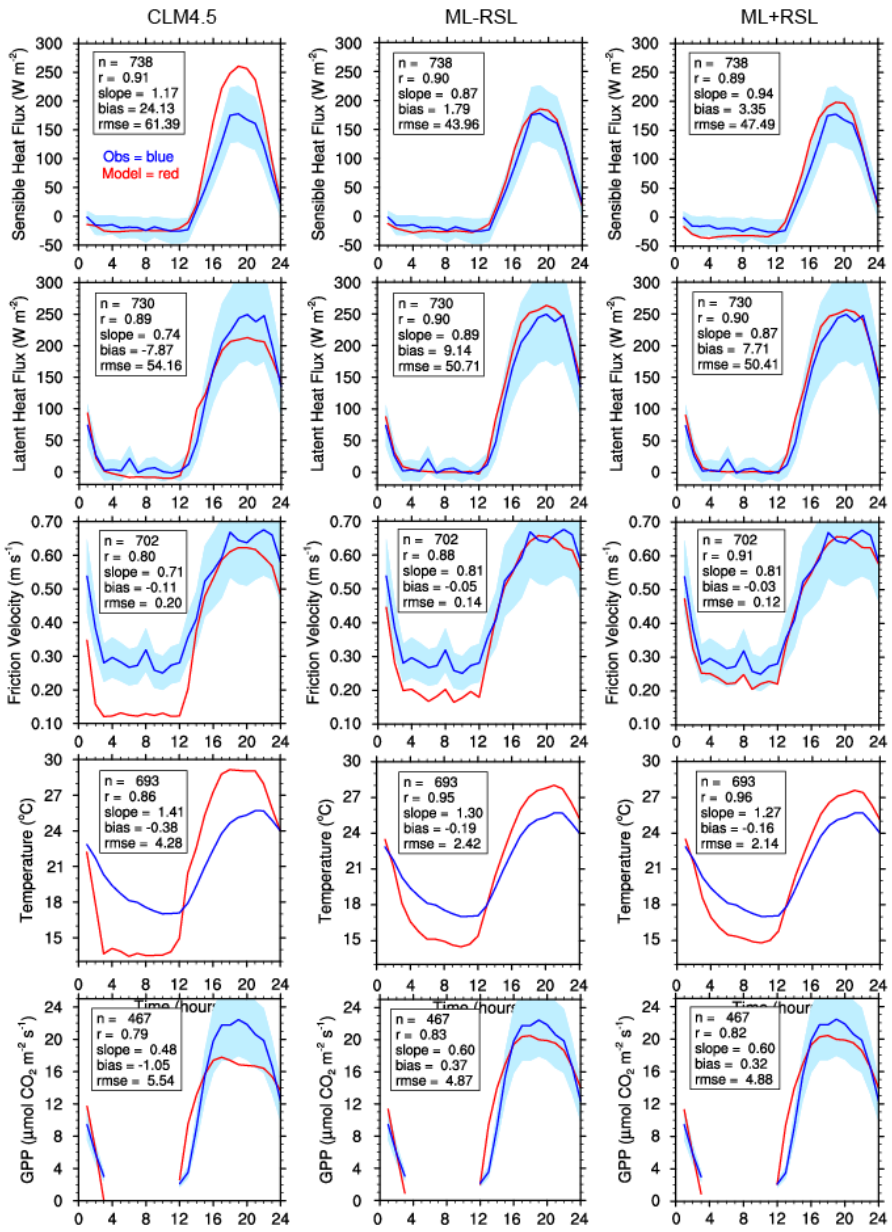
CLM4.5
ML-RSL
ML+RSL
Sensible Heat Flux (W m-2)
n = 738
r = 0.91
slope = 1.17
bias = 24.13
rmse = 61.39
Obs = blue
Model = red
n = 738
r = 0.90
slope = 0.87
bias = 1.79
rmse = 43.96
n = 738
r = 0.89
slope = 0.94
bias = 3.35
rmse = 47.49
Latent Heat Flux (W m-2)
n = 730
r = 0.89
slope = 0.74
bias = -7.87
rmse = 54.16
n = 730
r = 0.90
slope = 0.89
bias = 9.14
rmse = 50.71
n = 730
r = 0.90
slope = 0.87
bias = 7.71
rmse = 50.41
Friction Velocity (m s-1)
n = 702
r = 0.80
slope = 0.71
bias = -0.11
rmse = 0.20
n = 702
r = 0.88
slope = 0.81
bias = -0.05
rmse = 0.14
n = 702
r = 0.91
slope = 0.81
bias = -0.03
rmse = 0.12
Temperature (°C)
n = 693
r = 0.86
slope = 1.41
bias = -0.38
rmse = 4.28
n = 693
r = 0.95
slope = 1.30
bias = -0.19
rmse = 2.42
n = 693
r = 0.96
slope = 1.27
bias = -0.16
rmse = 2.14
GPP (µmol CO2 m-2 s-1)
n = 467
r = 0.79
slope = 0.48
bias = -1.05
rmse = 5.54
n = 467
r = 0.83
slope = 0.60
bias = 0.37
rmse = 4.87
n = 467
r = 0.82
slope = 0.60
bias = 0.32
rmse = 4.88

1291

Figure 4. Simulations for US-UMB (July 2006). Shown are the average diurnal cycle (GMT) of sensible heat flux, latent heat flux, friction velocity, radiative temperature, and gross primary production (GPP) for the observations (blue) and models (red). The shading denotes ± 1 standard deviation of the random flux error (Richardson et al., 2006, 2012) for H and λE and ± 20% of the mean for GPP and u_*. Statistics show sample size (n), correlation coefficient (r), slope of the regression line, mean bias, and root mean square error (rmse) between the model and observations. Left column: CLM4.5. Middle column: ML-RSL. Right column: ML+RSL.

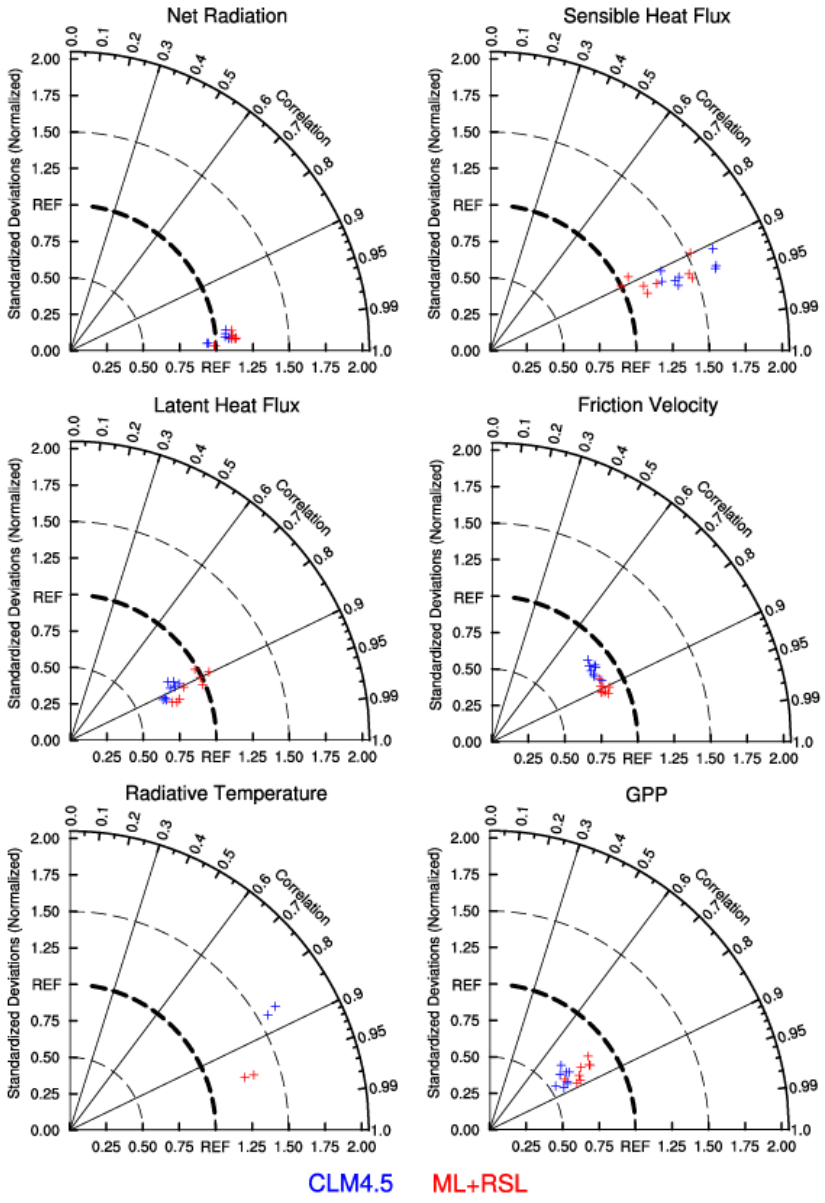
Net Radiation
Sensible Heat Flux
Latent Heat Flux
Friction Velocity
Radiative Temperature
GPP
Standardized Deviations (Normalized)
Correlation
REF
CLM4.5
ML+RSL

1301

Figure 5. Taylor diagram of net radiation, sensible heat flux, latent heat flux, friction velocity, radiative temperature, and gross primary production (GPP) for US-UMB. Data points are for the years 1999–2006 for CLM4.5 (blue) and ML+RSL (red). Simulations are evaluated by the normalized standard deviation relative to the observations (given by the radial distance of a data point from the origin) and the correlation with the observations (given by the azimuthal position). The thick dashed reference line (REF) indicates a normalized standard deviation equal to one. Model improvement is seen by radial closeness to the REF line and azimuth closeness to the horizontal axis (correlation coefficient equal to one).

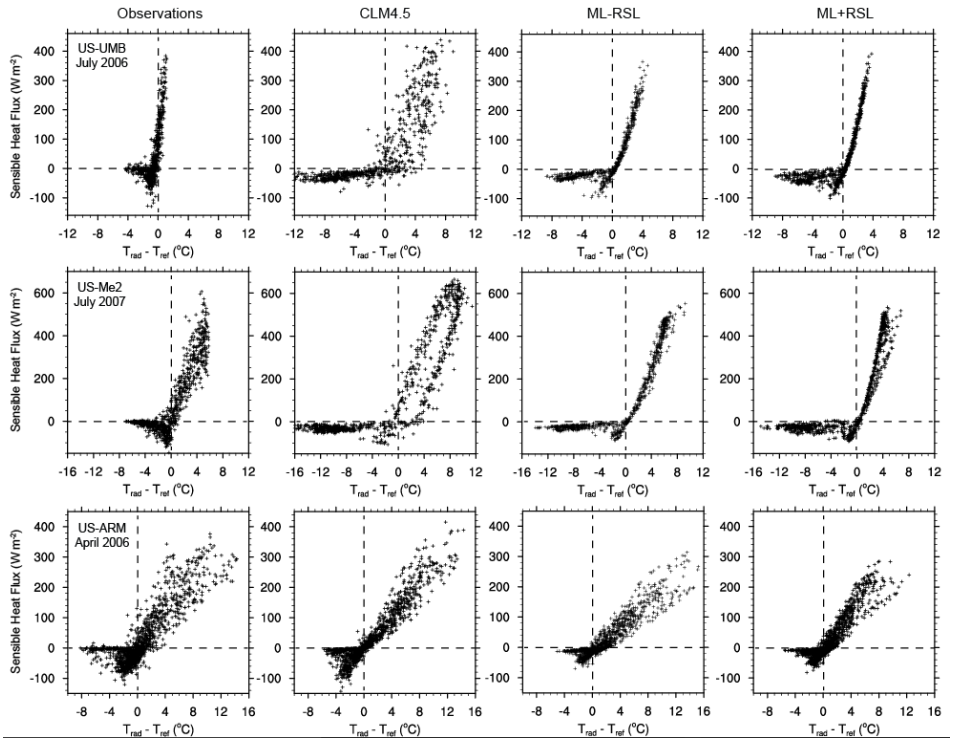

Figure 6. Sensible heat flux in relation to the temperature difference $T_{rad} - T_{ref}$ for US-UMB (July 2006), US-Me2 (July 2007), and US-ARM (April 2006). Shown are the observations (left column) and model results for CLM4.5, ML-RSL, and ML+RSL.

Deleted: Left column: Observations. Middle column: CLM4.5. Right column: ML+RSL.

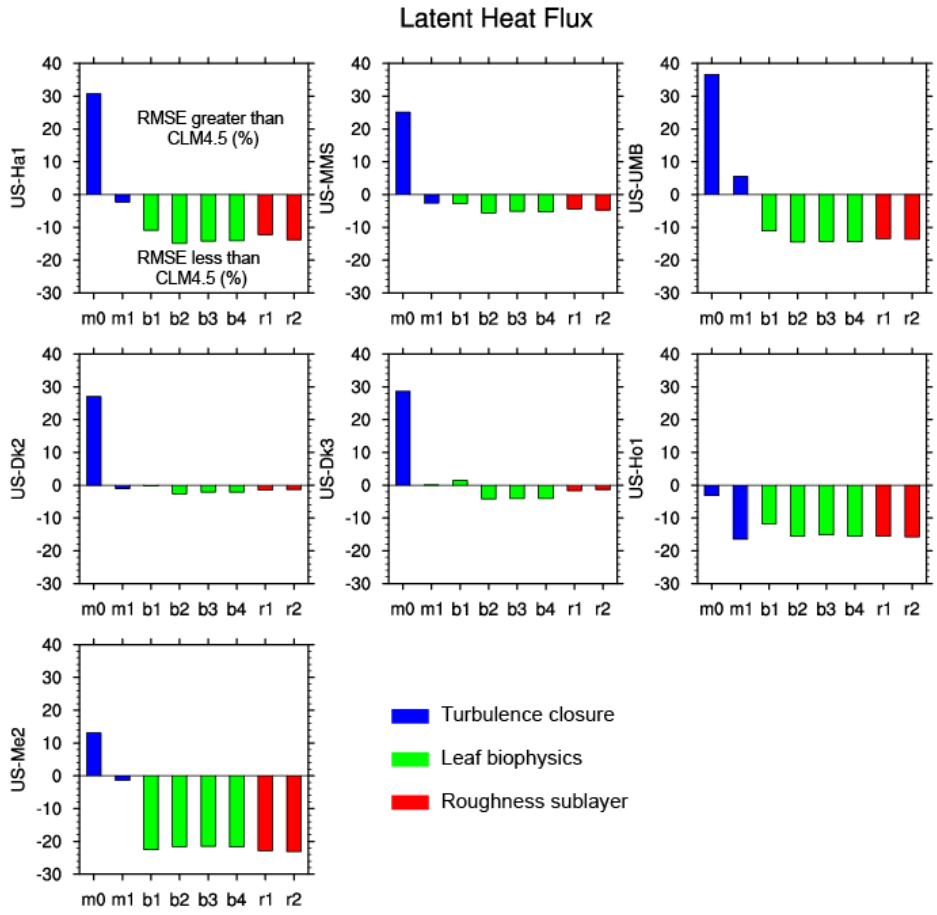

Figure 7. Root mean square error (RMSE) for latent heat flux for the 8 simulations m0–r2. RMSE for each simulation is given as a percentage of the RMSE for CLM4.5 and averaged across all years at each of the 7 forest sites. A negative value shows a reduction in RMSE relative to CLM4.5 and indicates model improvement. Changes in RMSE between simulations show the effect of sequentially including new model parameterizations as described in Table 4.

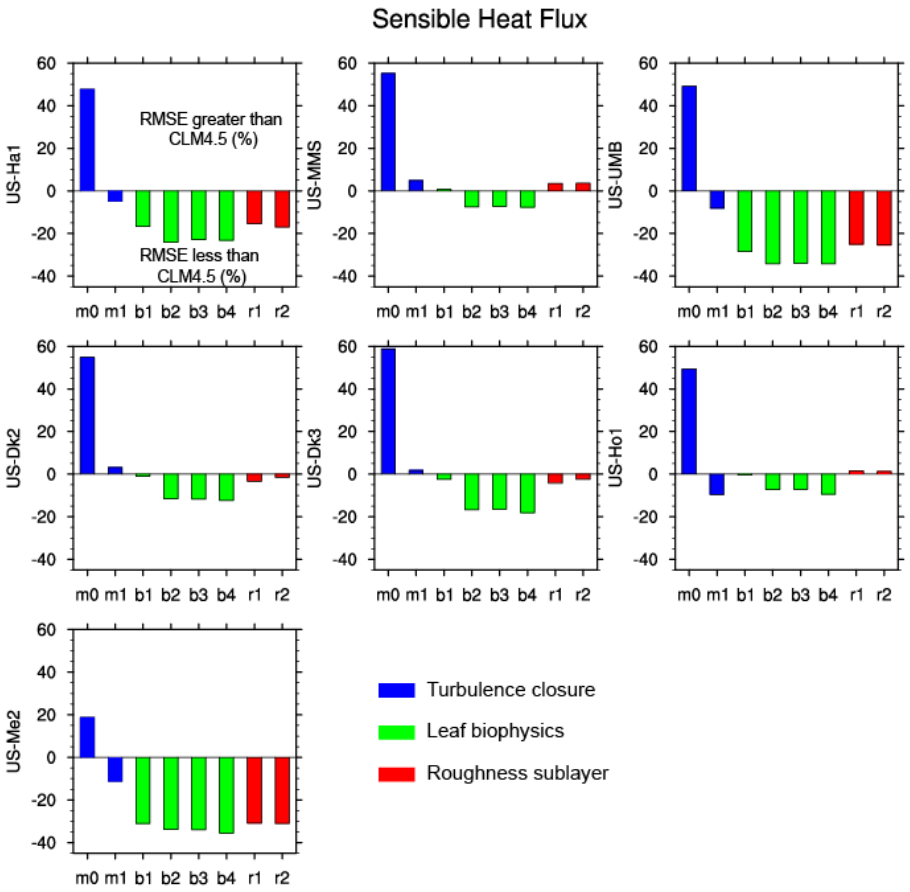

Figure 8. As in Figure 7, but for sensible heat flux.

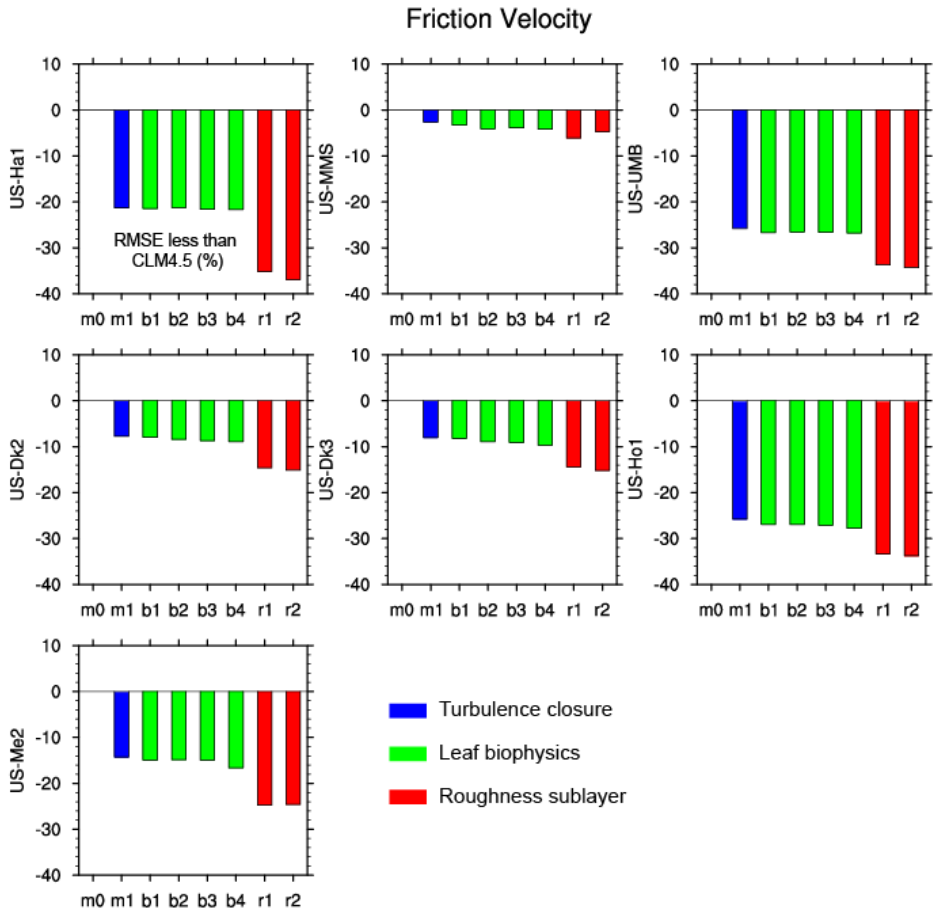

Figure 9. As in Figure 7, but for friction velocity.

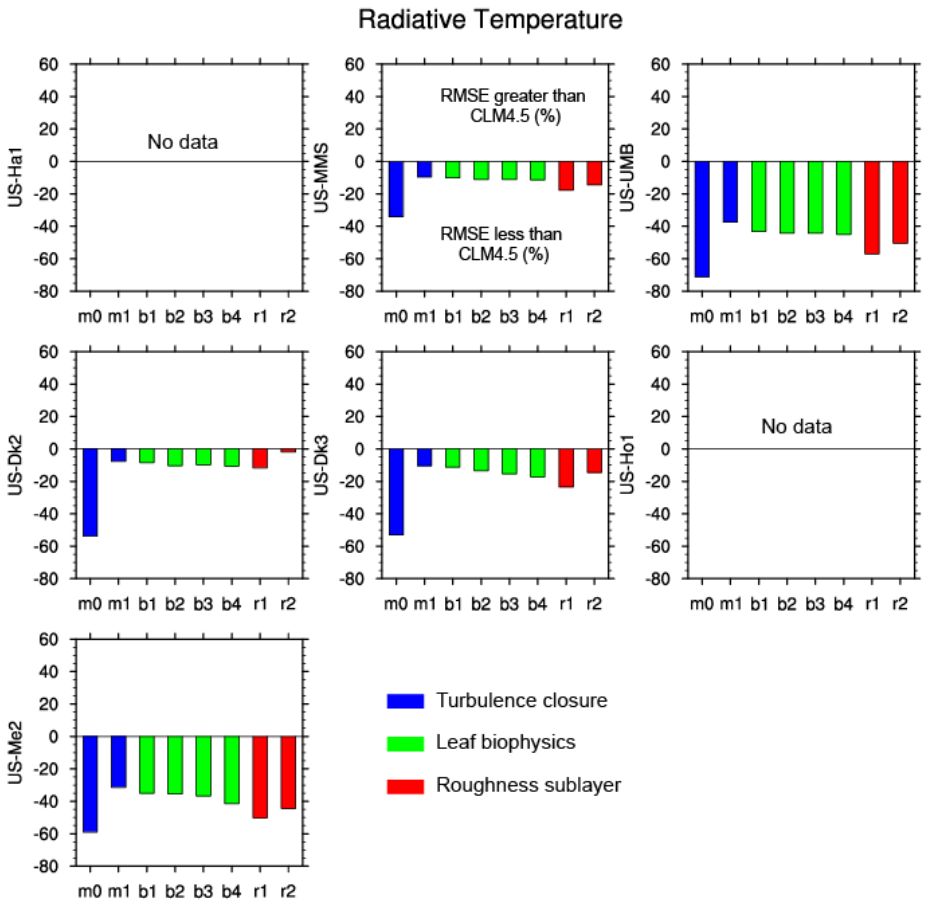

Figure 10. As in Figure 7, but for radiative temperature.

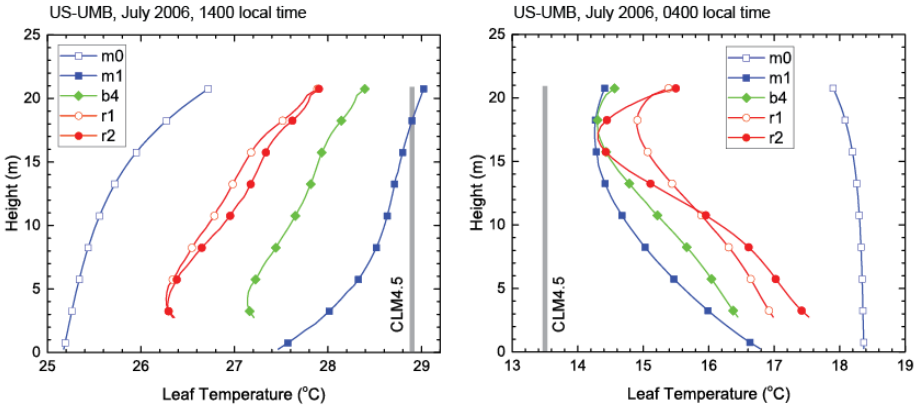

Figure 11. Profiles of leaf temperature for US-UMB averaged for the month of July 2006 at 1400 local time (left panel) and 0400 local time (right panel). Temperature is averaged for sunlit and shaded leaves at each level in the canopy. Shown are the m0, m1, b4 (ML-RSL), r1, and r2 (ML+RSL) simulations. The CLM4.5 canopy temperature is shown as a thick gray line, but is not vertically resolved.

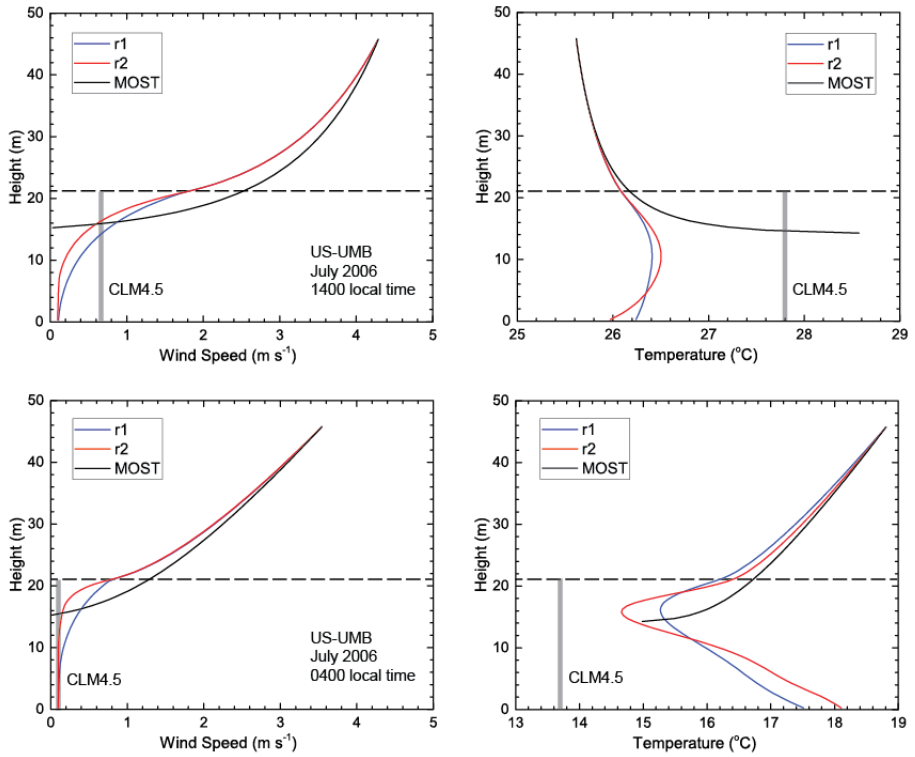

Figure 12. Profiles of wind speed and air temperature for US-UMB (July 2006) at 1400 local time (top panels) and 0400 local time (bottom panels). Shown are the r1 and r2 simulations averaged for the month. The dashed line denotes the canopy height. The CLM4.5 canopy wind speed and air temperature are shown as a thick gray line, but are not vertically resolved. Also shown are the profiles obtained using MOST extrapolated to the surface. This extrapolation is for the r2 simulation using Eqs. (19) and (20) but without the RSL and with roughness length and displacement height specified as in the CLM4.5.